Sediment melting during subduction initiation: Evidence of mantle-hosted S-type granitoids in the Neoproterozoic Fuchuan Ophiolite

Si-Fang Huang[1]*, Wei Wang[2]*, Andrew C. Kerr[3], Peter A. Cawood[4], Guimei Lu[5]

[1]*Henan Engineering Technology Research Center of Ecological Protection and Management of the Old Course of Yellow River, School of Surveying and Planning, Shangqiu Normal University, Shangqiu 476000, China.*
[2]*School of Earth Sciences, State Key Laboratory of Geological Processes and Mineral Resources, China University of Geosciences, Wuhan 430074, China*
[3]*School of Earth and Environmental Sciences, Cardiff University, Cardiff, CF10 3AT, UK*
[4]*School of Earth, Atmosphere and Environment, Monash University, Clayton, VIC 3800, Australia*
[5]*State Key Laboratory of Isotope Geochemistry, Guangzhou Institute of Geochemistry, Chinese Academy of Sciences, Guangzhou 510640, China*

***Corresponding author at:** School of Surveying and Planning, Shangqiu Normal University, Shangqiu 476000, China. Email address: **hsifang@sqnu.edu.cn**; School of Earth Sciences, China University of Geosciences, Wuhan 430074, China. Email address: **wwz@cug.edu.cn**

Abstract

The mechanisms and geodynamic significance of sediment recycling in subduction zones remain intensely controversial in Precambrian geology. This study reports a suite of Precambrian sediment-derived felsic intrusions preserved within an exhumed mantle peridotite of a supra-subduction zone in South China. These felsic rocks intruded into the peridotite of the Fuchuan Ophiolite show U-Pb ages of 846 - 837 Ma, coinciding with the dating of ca. 848 - 820 Ma crustal section rocks of the ophiolite, implying their generation during slab subduction rather than later obduction. Petrography, zircon O isotopic and trace elemental signatures of the Fuchuan mantle-hosted granitoids indicate S-type affinity. Integrated O ($\delta^{18}O$ = 7.5 ‰ to 11.3 ‰), Hf ($\varepsilon_{Hf(t)}$ = -3.8 to +6.9) and Nd ($\varepsilon_{Nd(t)}$ = -2.2 to -0.4) isotopic compositions, coupled with inherited zircon ages and whole-rock geochemistry, collectively suggest derivation from a continental margin sediment protolith. Geochemical analyses and pseudosection modeling reveal partial melting of subducted sediment at 650 - 790 °C and <4 kbar (~12-15 km). This condition of melting is atypical in a mature subduction channel, but is plausible during the initiation phase of subduction. Consequently, the mantle-hosted S-type intrusions formed during slab subduction may represent a proxy for subduction initiation. In contrast to the formation depth (< 14 kbar; depths < 45 km) of Phanerzoic mantle-hosted leucogranitoids, sediment-derived melt transport from subducting slabs during the Neoproterozoic occurred at substantially shallower depths, suggesting that the Neoproterozoic era may witness the reoperating of modern-style plate tectonics after Earth's middle age, occurring under elevated mantle potential temperatures relative to present-day conditions.

Keywords: mantle-hosted S-type granitoids, Neoproterozoic, South China, subduction initiation, plate tectonics

1. Introduction

Subduction is the main mechanism of mass transfer from Earth's surface to its mantle and has the potential to modify the compositions of mantle, crust, hydrosphere, and atmosphere (Klaver et al., 2024; Stern, 2002; Zheng, 2019; Zheng et al., 2019). Sediments, containing abundant lithophile elements (for example, K, Rb, Th, U and LREE), play a pivotal role in the generation of volcanic arc magmas and the crust-mantle interaction processes during slab subduction (Klein and Behn, 2021). In the classic model, sediments on top of the subducting slab release aqueous fluids and melts, which metasomatize the mantle peridotite and thus facilitate the generation of mantle-derived magma (Li et al., 2022; Zheng, 2019). However, some recent studies have revealed that oceanic sediments, altered basaltic crust and serpentinite from the subducted slab can potentially ascend as a diapiric fashion into the overlying mantle wedge (Behn et al., 2011). Although slab subduction has been recognized from the early Neoproterozoic and even the Archean (Zheng and Zhao, 2020), critical geological evidence is lacking on whether sediment transfer conditions in Precambrian subduction zone matched that in Phanerozoic, given the differences in thermal state between the Precambrian and contemporary Earth (van Keken et al., 2018).

Suprasubduction zone (SSZ) ophiolites comprise fragments of oceanic crust and underlying mantle rocks and represent key archives for investigating mass transfer and crust-mantle interactions in subduction systems (Cawood et al., 2024; Stern, 2002). Granitic rocks within oceanic crustal units of the SSZ-type ophiolites are commonly plagiogranites, generated through fractional crystallization of mantle-derived melts or partial melts of oceanic crust (Çörtük et al., 2024; Li et al., 2022a, 2023; Sun et al., 2020). Meanwhile, a minor proportion of peraluminous granitoids within the ophiolite are genetically linked to the partial melting of metasedimentary rocks during obduction (Cox et al., 1999; Li et al., 2008). However, mantle-hosted S-type granitoids within the SSZ-type ophiolite formed during slab subduction, although rare, preserve a record of direct melting of sediment at mantle depths and thus crustal-mantle interaction during slab subduction (Angelo et al., 2023; Haase et al., 2015). As a result, deciphering the petrogenesis of mantle-hosted S-type granitoids can be potentially used to understand the mechanism of sediment transfer and subduction zone crust-mantle interaction. At present, the mantle-hosted S-type granitoids formed during the process of oceanic slab subduction have predominantly been reported from the Phanerozoic Samail Ophiolites (Angelo et al., 2023; Cox et al., 1999; Rioux et al., 2021), whereas their counterparts in Precambrian ophiolites have rarely been documented (Huang et al., 2021).

In this work, we report Neoproterozoic mantle-hosted S-type intrusions from the SSZ-type Fuchuan Ophiolite, South China (Fig. 1). Field and petrological observations, whole-rock geochemistry and Nd isotope, zircon trace elements, zircon U-Pb geochronology and Hf-O isotopes of these mantle-hosted S-type intrusions indicate generation by partial melting of sediment in a subduction channel, and subsequent intrusion into the cold corner of the mantle wedge. Temperature and pressure estimates suggest that mantle-hosted S-type granitoids in ophiolites may be a proxy for subduction initiation. In addition, our findings indicate that during the Neoproterozoic era, the depth at which sediments were transported from subducting slabs into the mantle was significantly shallower than observed in modern subduction systems.

2. Geological background

The Neoproterozoic Fuchuan Ophiolite lies in the eastern part of the Jiangnan Belt of South China (Bai et al., 1986; Zhao, 2015; Zhou et al., 1989; Zhou and Zhao, 1991). The ophiolite comprises serpentinized harzburgite with minor pyroxenite, dunite, wehrlite, lenses of chromitite and veins (or blocks) of granitoids in its mantle section. Its crustal section consists of isotropic gabbro (with subordinate layered troctolite and anorthosite), pillowed lava and sedimentary cover (including black chert, metagraywacke and tuffaceous sandstone) (Fig. 1; Bai et al., 1986; Zhang et al., 2012). Zircon U-Pb geochronology, whole-rock and mineral geochemistry suggest that the Fuchuan Ophiolite formed at ca. 848 - 820 Ma in a suprasubduction zone (SSZ) setting (Huang et al., 2021; Li and Zhao, 2020; Shu et al., 2019; Zhang et al., 2013). The Fuchuan Ophiolite was obducted into the early Neoproterozoic littoral- to marine-facies autochthonous sedimentary sequences of the Shangxi/Xikou Group and onto the Shexian granitoid plutons after ca. 820 Ma, with mylonitization occurring along the thrust-fault contact zone (Ding et al., 2008; Li et al., 2003; Wang et al., 2013a; Yao et al., 2019). The SE-dipping mylonitic foliations are pervasively developed in both the Shangxi/Xikou Group and the Shexian granitoid plutons, indicating that the Fuchuan Ophiolite was emplaced as a tectonic nappe from southeast to northwest direction (Bai et al., 1989; Ding et al., 2008; Zhou et al., 1989).

The Shangxi/Xikou Group was mainly derived from the Neoproterozoic magmatic arc with a peak U-Pb zircon age of 830 - 1000 Ma and so the maximum depositional age has been interpreted to be ca. 820 - 830 Ma (Wang et al., 2013a; Xu et al., 2014). The Shexian granitoid plutons, along with the Xucun and Jiuling plutons in the Jiangnan Belt, are markedly strongly peraluminous (Huang et al., 2025; Li et al., 2003; Shen et al., 1993; Wu et al., 2006; Xu and Zhou, 1989; Zheng et al., 2008). These plutons have been dated at ca. 850 - 810 Ma, and may have formed in a syn-/post-collisional tectonic setting when the Yangtze and Cathaysia Blocks amalgamated (Li et al., 2003; Wu et al., 2006; Wang et al., 2013b, 2023; Zheng et al., 2008). Alternatively, they have been interpreted as being generated in a back-arc extension setting when the paleo-Huanan oceanic slab subudcted along the southeastern margin of the Yangtze Block (Yao et al., 2019; Zhu et al., 2023; Huang et al., 2025). These peraluminous granitoid plutons and sedimentary sequences, along with the Fuchuan Ophiolite, are unconformably overlain by the late Neoproterozoic sedimentary sequences formed during Nanhua rifting (Wang et al., 2016; Yin et al., 2013).

Numerous felsic intrusions, varying in width from 0.1 to 2 meters, intrude the harzburgite matrix of the Fuchuan Ophiolite, without any discernible metamorphic aureole or mylonitization in the contact zone (Fig. 1d-f). These felsic intrusions exhibit tectonic dislocation, with their shear sense aligned with the mylonitized foliation orientation in the thrust-fault contact zone, demonstrating they constitute a part of the Fuchuan Ophiolite (Shu et al., 2019). In contrast to country granitoids, exemplified by the Shexian granitoid plutons, which are typically characterized by enrichment in mafic minerals (~10 - 20%; Fig. 1g), the felsic intrusions, intruded into harzburgite of the Fuchuan Ophiolite, exhibit an off-white coloration and lack significant mafic mineral content (colour index < 5; Fig. 1f). Therefore, the felsic intrusions of the Fuchuan Ophiolite are known as Fuchuan mantle-hosted granitoids to distinguish them from the country granitoid rocks (e.g., Shexian granitoid pluton). They are mainly composed of potassium feldspar (30 - 40 vol.%), plagioclase (20 - 25 vol.%), quartz (10 - 30 vol.%), muscovite (~5 vol.%) and accessory minerals (cordierite, zircon, and apatite) (Fig. 1h-i). In contrast to typical plagiogranites, marked by plagioclase enrichment, the Fuchuan mantle-hosted granitoids are characterized by their abundance of potassium feldspar (Fig. 1h-i).

3. Methods

Zircon cathodoluminescence images were acquired at the State Key Laboratory of Geological Process and Mineral Resources (GPMR), with a CL 4+ system integrated into a Zeiss Sigma 300 scanning electron microscope. *In-situ* zircon O isotope analyses were measured using the Cameca IMS-1280 SIMS housed at Guangzhou Institute of Geochemistry following the analytical procedures given in Li et al. (2010). The standard zircon Qinghu was as an unknown sample to monitor data quality, yielding weighted mean value of $\delta^{18}O$ is 5.55 ± 0.12‰ (2σ, n=13), which is identical to the reported value of 5.46‰ ± 0.24‰ within the errors (Yang et al., 2018). *In-situ* zircon U-Pb dating were determined using an Agilent Technologies 7700x quadrupole ICP-MS were attached with RESOlution laser-ablation system at GPMR. Zircon 91500 was set as external standard material. Zircon GJ-1 and Plešovice were used as unknown samples to monitor quality of geochronology with weighted mean $^{206}Pb/^{238}U$ ages of 599.4 ±3.6 Ma (MSWD= 3.0, n = 14) and 337.0 ±2.8 Ma (MSWD = 0.64, n = 7), respectively (Jackson et al., 2004; Sláma et al., 2008). Trace elemental contents of zircon were calibrated using ^{29}Si as internal standard and NIST SRM 610 as an external reference standard material. Zircon Lu-Hf isotope analyses were measured at GPMR, using a Neptune Plus multi-collector ICP-MS attached with an ArF excimer laser ablation system. Standard zircon 91500 and GJ-1was used for quality control. Raw datasets of zircon U-Pb and Lu-Hf isotopes were processed using *ICPMSDataCal* software (Liu et al., 2010). Concordia diagrams and age calculation were performed on-line by procedure of *IsoplotR* (Vermeesch, 2018).

Whole-rock major element compositions were obtained at GPMR using a Shimadzu 1800-XRF. Measurements of trace element abundances were conducted using an Agilent 7700x ICP-MS at Nanjing FocuMS Technology Co. Ltd. The sample was firstly digested by acetic acid, and then by HF + HNO_3 mixture at 190 °C for 48 h to ensure complete dissolution of residue. Pure elemental standards were used as external calibration for instrument responses and internal reference materials BHVO-2, W-2, GSP-2 and AGV-2 were used to monitor the quality of analyses. High precision radiogenic Nd isotope composition was measured by Nu Instruments Plasma II MC-ICP-MS. Detailed analytical procedures were described by Chen et al. (2009).

Pseudosection modeling was carried out by GeoPS (http://www.geops.org/zh-cn/) with the MnNCKFMASHT system and employed the hp633ver.dat thermodynamic database (Xiang and Connolly, 2022). The a-x solution models for orthopyroxene [Opx(W)], garnet [Gt(W)], melt [melt(W)], mica [Mica(W)], ilmenite [Ilm(W)], cordierite [Crd(W)], biotite [Bi(W)], chlorite [Chl(W)], chloritoid [Ctd(W)] and spinel [Sp(WPC)] from White et al. (2014), and for feldspar [Fsp(C1)] and epidote [Ep(HP11)] from Holland and Powell (2011) were used. The modeling focused on the Xikou Group metasedimentary rocks, assuming an $Fe^{3+}/(Fe^{3+}+Fe^{2+})$ ratio equivalent to 0.1.

4. Results

4.1. Zircon U-Pb geochronology

While a few zircon grains from the Fuchuan mantle-hosted granitoids have core-rim structure, most of them show clear oscillatory zoning (Fig. 2a-d). Zircons from the studied grains have Th/U ratio ranging from 0.11 to 1.32, total REE concentrations of 310 - 3486 ppm, positive Ce (Ce/Ce* = 1 - 395) and negative Eu anomalies (Eu/Eu* = 0.02 - 0.51), indicative of magmatic origin (Fig. S1). High $(Sm/La)_N$, consistent $(Yb/Dy)_N$ values and lack of correlation between Th/U and LREE-I [LREE-I = (Dy/Nd)+(Dy/Sm)] values (Fig. S1), also suggest the zircons of the felsic intrusions are magmatic (Bell et al., 2016). A total of 120 zircon spots from 4 samples for U-Pb dating were measured. Twenty-seven of them show older $^{206}Pb/^{238}U$ apparent ages, varying from 880 to 2468 Ma, and are considered as xenocrysts from the source material rather than captured from wall rocks, because the studied intrusions outcrop in mantle peridotite (Fig. 1d, e). Nine spots were analyzed on the zircon cores with ages ranging from 829 to 852 Ma, and they are also considered to be xenocrysts, because of the inconsistent oscillatory zoning in the core and the rim, and low U contents (Figs. 2 and

S1). Eleven zircon grains with younger ages of 646 to 806 Ma are dark and have high U contents, indicative of a later thermal event (Bell et al., 2016). Sixteen zircon grains show discordant U-Pb ages, attributed to later lead loss (Bell et al., 2016). The remaining analyses for samples FC19-21, FC19-22, FC10-01 and FC10-36 yield $^{206}Pb/^{238}U$ weighted mean ages of 842 ± 4 Ma (MSWD = 1.06, n = 17), 844 ± 5 Ma (MSWD = 1.20, n = 15), 845 ± 5 Ma (MSWD = 0.77, n = 14) and 846 ± 4 Ma (MSWD = 0.76, n = 12), respectively (Fig. 2e-h). These ages, within analytical uncertainty, agree with previous LA-ICP-MS/SIMS zircon ages (841 ± 5 Ma; 840 ± 5 Ma and 837 ± 6 Ma) for the Fuchuan mantle-hosted granitoids (Li and Zhao, 2020; Shu et al., 2019) and are interpreted as the emplacement age. Existing studies document that mafic-ultramafic magmatism (e.g., gabbros, anorthosites, wehrlites) in the Fuchuan Ophiolite persisted from ca. 848 Ma to ca. 820 Ma (Huang et al., 2021 and references there in), indicating that the Fuchuan mantle-hosted granitoids (ca. 846 - 837 Ma) formed during oceanic slab subduction rather than during obduction of the ophiolitic suit onto the continental margin.

4.2. Zircon Hf-O isotopes

Magmatic zircons exhibit elevated $\delta^{18}O$ values ranging from 7.47 ± 0.23 ‰ to 11.27 ± 0.29 ‰ (n = 36), averaging 9.16 ± 0.26 ‰ (2σ; Fig. S2). In contrast, inherited zircon grains display significantly greater $\delta^{18}O$ variability (4.70 ± 0.16‰ to 10.35 ± 0.22‰, n = 27), with their oxygen isotope composition characterized by a distinct bimodal distribution pattern (Fig. S2). The $\varepsilon_{Hf(t)}$ values of magmatic (n = 51) and inherited (n = 27) zircons range from -3.8 ± 0.5 to +6.9 ± 0.5 and from -4.9 ± 0.5 to +13.0 ± 0.7, respectively.

4.3. Whole-rock geochemistry and Nd isotopes

The Fuchuan mantle-hosted granitoids display variable SiO_2 (62.7 - 75.1 wt. %), K_2O (4.3 - 9.1 wt. %), Na_2O (2.4 - 6.8 wt. %) and Al_2O_3 (12.7 - 16.7 wt. %) contents, and high K_2O/Na_2O ratios (0.71 - 3.09; Fig. 3). Aluminum saturation index (ASI) of the Fuchuan mantle-hosted granitoids range from 0.65 to 1.04, which may represent an underestimate due to the presence of calcite veins (width of ~1 mm) in felsic intrusions.

These mantle-hosted granitoids have crust-derived rather than mantle-derived granite (e.g. plagiogranite in ophiolite) features, including fractionated light rare earth elements [$(La/Sm)_N$ = 1.48 - 2.83], unfractionated heavy rare earth element patterns [$(Dy/Yb)_N$ = 0.84 - 1.12], and significantly negative Eu anomalies (Eu/Eu* = 0.16 - 0.42; Fig. 4a). Pronounced enrichment of LILEs (Rb, U, K and Pb) and depletion of HFSEs (Nb, Ta and Ti) related to primitive mantle are also indicative of crustal origin of the magma (Fig. 4b).

The Fuchuan mantle-hosted granitoids have measured $^{143}Nd/^{144}Nd$ ratios ranging from 0.512265 to 0.512615, and the corresponding whole-rock $\varepsilon_{Nd(t)}$ values from -2.2 to -0.4.

5. Discussion

5.1. Fuchuan mantle-hosted granitoids derived from partial melts of subducted sediments

Investigations relying exclusively on zircon U-Pb-Hf isotopic data propose that the Fuchuan mantle-hosted granitoids are mantle-derived plagiogranites (Li and Zhao, 2020; Shu et al., 2019). However, we demonstrate that these granitoids show features of S-type granites, including high K_2O contents and the presence of magmatic muscovite, cordierite, and abundant inherited zircons. The $\delta^{18}O$ values (7.5 ‰ - 11.3 ‰) of magmatic zircons are higher than both mantle and lower crustal values (5.3 ± 0.6 ‰) (Valley et al., 2003), thus suggesting their supracrustal material source. Phosphorus content of the studied magmatic zircons is highly variable (208 to 2369 ppm; 76 % grains > 600 ppm), with a mean concentration of 1136 ± 596 ppm, similar to zircons from the Lachlan S-type granites (1000 ± 490 ppm) (Burnham and Berry, 2017). The REE + Y contents of zircon positively correlate with P concentrations, with a slope of 1, further indicative of a S-type granite affinity (Fig. 5a). This conclusion is demonstrated by the cumulate curves of P and Y contents and U/Th ratios of zircon (Fig. 5b). Furthermore, there is a close similarity in trace element patterns between the Fuchuan mantle-hosted granitoids and leucogranites from the Samail Ophiolite and the Himalayas (Fig. 4).

The intrusion of Fuchuan mantle-hosted granitoids into a matrix of mantle peridotite, means that it is possible that the native mantle constituents imparted a significant chemical imprint upon the Fuchuan felsic intrusions. However, low MgO (0.4 - 2.2 wt. %), Cr (mean of 17 ppm), and Ni (mean of 21 ppm) contents of the Fuchuan mantle-hosted granitoids suggest negligible mantle contribution. This is also supported by the sharp contact (without any discernable contact metamorphic aureole) between felsic intrusions and harzburgite. The lack of disequilibrium mineral pairs precludes the possibility of crustal-mantle hybrids (Sylvester, 1998), and this is also supported by their consistent La/Sm (2.3 - 4.4) ratios and $\varepsilon_{Nd(t)}$ (-0.4 to -2.2) values. A notable feature of the Fuchuan mantle-hosted granitoids is the pronounced decoupling between the predominantly positive $\varepsilon_{Hf(t)}$ (up to +6.9) and the negative whole-rock $\varepsilon_{Nd(t)}$ values. The presence of inherited zircons indicates zirconium saturation in the melt, implying that residual zircons were preserved in the source. These zircons retained Hf-Nd fractionation signatures during partial melting, as reflected by the low Hf contents (2.42 - 4.39 ppm) and high Nd/Hf ratios (1.72 - 6.20) of the Fuchuan mantle-hosted granitoids. We suggest that these residual zircons sequestered substantial ^{177}Hf in the source, thereby elevating the $\varepsilon_{Hf(t)}$ values of the derived melt and decoupling it from the $\varepsilon_{Nd(t)}$. Batch partial melts derived from crustal sources can exhibit a wide spectrum of $\varepsilon_{Hf(t)}$ values (Tang et al., 2014). Therefore, the Hf isotopic heterogeneity observed in the Fuchuan mantle-hosted granitoids likely originated from mixing of multiple melt batches derived from a common source, rather than from mixing between mantle- and crust-derived magmas. Meanwhile, the positive correlation between $\varepsilon_{Hf(t)}$ and δ^{18}O of magmatic zircons does not support two end-member mixing, ruling out a significant mantle-derived material contribution (Fig. 6a). Furthermore, a significant contribution of mantle-derived melts would yield high Na_2O contents and consequent low K_2O/Na_2O ratios, which is inconsistent with the Fuchuan mantle-hosted granitoids (Fig. 3). Therefore, we argue that the Fuchuan mantle-hosted granitoids were derived from the partial melting of subducted sediments with insignificant contribution from the mantle peridotite.

5.2. Continental margin sediments as the magma source for the Fuchuan mantle-hosted granitoids

Sediments subducted into the mantle on a down going oceanic plate can be abyssal or continental margin in origin. Abyssal sediments are mainly composed of pelagic mud, and siliceous and carbonate oozes. The moderate-to-high paleo-latitudinal positioning of the Yangtze Block within Rodinia (de Kock et al., 2024), along with the comparatively limited faunal distribution during the early Neoproterozoic era (before 850 Ma) (Retallack, 2013), means that carbonate ooze and its counterparts are not effective candidates for melting to produce the Fuchuan mantle-hosted granitoids. The δ^{18}O values (7.5 ‰ - 11.3 ‰) of magmatic zircons from the Fuchuan mantle-hosted granitoids are significantly lower than leucogranite ($\delta^{18}O$ up to 26 ‰) derived from pelagic mud in Samail Ophiolite (Spencer et al., 2017). The melt of siliceous rock would have extremely high SiO_2 contents (> 80 wt.%) as compared to mantle-hosted granitoids. Calculations shows that even with 1 % partial melting of global subducting sediment (GLOSS) and typical abyssal metasediments (from Samail Ophiolite), the melts would still show significantly low Th/La ratios (0.37 and 0.58, respectively) relative to the Fuchuan mantle-hosted granitoids (0.48 - 1.27; Fig. 7). All the above observations indicate that abyssal sediment was not the melt source of the Fuchuan mantle-hosted granitoids.

The Fuchuan mantle-hosted granitoids exhibit Sm/La and Th/La ratios comparable to those observed in Himalayan leucogranites and $\varepsilon_{Hf(t)}$ - $\delta^{18}O$ values of magmatic zircons to the ca. 850 - 810 Ma S-type granitoids in the Jiangnan Belt (Figs. 6-7), suggesting continental metasedimentary rocks are the primary magma source. Calculation of Hf-O isotopes suggests that the sedimentary source of the Fuchuan mantle-hosted granitoids contained ~30% to 80% juvenile crust components, which is also supported by ~50% inherited zircons with mantle-type $\delta^{18}O$ values (Fig. 6a). This juvenile signal was likely inherited from adjacent juvenile arc crust (e.g., the Jiangnan arc) that supplied detritus to the sedimentary source, as most inherited zircons with $^{206}Pb/^{238}U$ ages ranging from 1000 Ma to 930 Ma are coeval with arc-related magmatism in the eastern segment of the Jiangnan Belt (Yao et al., 2019 and references therein). Furthermore, the studied mantle-hosted granitoids have whole-rock $\varepsilon_{Nd(t)}$ values (-0.4 to -2.2) and two-stage Nd model ages (1.54 - 1.64 Ga) similar to the ca. 850 - 810 Ma strongly peraluminous granitoids (-3.0 to -0.3; 1.51 - 1.74 Ga) and the Shangxi/Xikou Group sediment sequences (+0.1 to -2.7; 1.38 - 1.63 Ga) in the Jiangnan Belt (Chen and Jahn, 1998; Li et al., 2003; Huang et al., 2019; Wu et al., 2006; Wang et al., 2016, 2023; Zheng et al., 2018; Zhu et al., 2023), confirming the continental margin sediments derived interpretation. This interpretation is supported by the presence of abundant inherited zircons, which mainly show Neoproterozoic U-Pb apparent ages (ca. 830 - 1000 Ma), similar to detrital zircon age patterns from the Neoproterozoic Shangxi/Xikou Group (Wang et al., 2013a).

5.3. Partial melts of subducted sediments during the incipient subduction

The Fuchuan mantle-hosted granitoids have low to medium Al_2O_3 contents (12.7-16.7 wt.%), strongly negative Eu anomalies (Eu/Eu* = 0.16 - 0.42), low Sr/Y ratios

(1.12-10.4) and flat HREE patterns ($(Dy/Yb)_N$ = 0.84-1.12; Fig. 4a), indicating that plagioclase instead of garnet was the dominant crystallizing/residual phase (Rioux et al., 2021). The constant Eu/Eu* values in these granitoids along with the variable Ba/Sr and Rb/Sr ratios (Fig. 8), show that plagioclase (as a residual phase) has played a key role in the magma source, indicating low-pressure partial melting in the plagioclase stability region (Zhu et al., 2023). Thermodynamic modeling of partial melting of metasedimentary rocks from the Shangxi/Xikou Group demonstrates that melts with elevated K_2O/Na_2O ratios (up to 2.1), comparable to those observed in the Fuchuan mantle-hosted granitoids, are generated under low-pressure conditions with insignificant garnet residue (< 4 kbar, corresponding to depths < 12 - 15 km) (Fig. 9a). Phase equilibrium analyses of the plagioclase-dominant and garnet-free source lithology under varying thermal regimes imply melting temperature for the generation of Fuchuan mantle-hosted granitoids below 800 °C, with requisite high geothermal gradients (Fig. 9b-c).

While evidence from thermobarometric modeling supports the possibility that the peraluminous granitoids within the ophiolite could have been derived from the melting of underlying sediments during obduction (Li et al., 2008; Whitehead et al., 2000), the geochronological results (846 - 837 Ma) indicate that the Fuchuan mantle-hosted granitoids were formed during oceanic slab subduction (this study; Li and Zhao, 2020; Shu et al., 2019). The temperature experienced by sediments at the top of subducted slab (< 2.0 GPa) in a normal subduction zone with arc magmatism is below 600 °C (Gerya, 2011; van Keken et al., 2018), much lower than the melt temperatures (657 - 785 °C) of the Fuchuan felsic intrusions estimated through Ti-in-zircon and zircon saturation geothermometer (Boehnke et al., 2013; Watson and Harrison, 2005). Numerical modeling indicates that the temperature within the mantle wedge near the trench can reach up to 800 °C (Gerya, 2011). Consequently, the diapir melting of mélange, which consists of sediment, altered oceanic crust, and mantle peridotite, could be a plausible mechanism for the formation of the Fuchuan mantle-hosted granitoids (Behn et al., 2011). Nevertheless, experimental petrology suggests that mélange-derived melts are generally metaluminous (A/CNK < 1.0), and are characterized by relatively low SiO_2 (49 - 58 wt. %), high MgO (1.0 - 16 wt. %) contents and low K_2O/Na_2O (< 0.5) ratios (Cruz-Uribe et al., 2018). Furthermore, the melts forming the Fuchuan mantle-hosted granitoids are pure sediment-derived melts (Fig. 3). Added to this, recent temperature-pressure experimental petrology shows that subduction zone mélange dehydration forms dense peridotite with buoyancy loss, inhibiting diapir ascent (Rebaza et al., 2024).

Alternatively, such high melting temperatures could be reached when subduction initiation, as the geotherms of subduction initiation are prone to be particularly steep in comparison with a mature subduction zone (Hall et al., 2003; Rollinson, 2015; van Keken et al., 2018). Considering the suprasubduction zone setting of the Fuchuan Ophiolite, together with the high-T and low-P conditions of the felsic melts, we propose that the mantle-hosted S-type granitoids were derived from partial melting of subducted sedimentary rocks during incipient subduction. Following this these S-type granitic melts would have been emplaced into the shallow and cold corner of mantle wedge forming through lithospheric extension of the upper plate in response to oceanic slab sinking (Fig. 10a). Therefore, such mantle-hosted S-type granitoids are an excellent proxy for modelling the process of subduction initiation.

The Fuchuan mantle-hosted granitoids can be modelled by partial melting of subducted sedimentary rocks and thus provide significant insight in deciphering the process of sediment recycling in the subduction zone and arc magmatism. Both the boninitic lavas and highly depleted mantle peridotites in the Fuchuan Ophiolite show significant enrichment in incompatible elements, including Rb, K, Th, U, and light rare earth elements (Huang et al., 2021; Li and Zhao, 2020; Zhao and Asimow, 2014). This distinct geochemical signature is remarkably similar to the enrichment patterns observed in the Fuchuan mantle-hosted granitoids (Fig. 4b). Furthermore, it is widely recognized that melts derived from subducted sediments play a crucial role in the generation of boninites, as evidenced by the well-studied examples from the Samail Ophiolite and the Izu-Bonin arc (Ishikawa et al., 2005; Li et al., 2022b). These phenomena collectively suggests that the Fuchuan mantle-hosted granitoids likely represent the subducted slab-derived component responsible for metasomatizing the mantle source region prior to boninitic magma generation. Therefore, with the further down-going of subducting slab after the generation of S-type felsic intrusions, sediment-derived melts metasomatize deeper and hotter mantle peridotite and then trigger boninitic melts (Fig. 10b). This model may offer new insights into the multistage island-arc subduction along the southeastern margin of the Yangtze Block during 1000 - 820 Ma (Chen, 1993; Guo et al., 1984; Shu et al., 1994, 2019; Wang et al., 2013a, 2013b; Yao et al., 2019; Zhao, 2015; Zheng et al., 2008).

5.4. Significance of subduction sediments recycling in Neoproterozoic

The mantle-hosted S-type granitoids in the Phanerozoic Samail Ophiolite have trace element geochemical signatures are similar to boninitic lavas derived from depleted mantle peridotites (Haase et al., 2015) and this provides further support for our subduction initiation model. However, these Phanerozoic mantle-hosted S-type granitoids show slight HREE depletion compared to the Fuchuan mantle-hosted granitoids (Fig. 4a). Calculations and thermodynamic modeling of Rioux et al. (2021) suggests that the sources of these Phanerzoic mantle-hosted granitoids have at least 5-10 % garnet, corresponding to a pressure of < 14 kbar (depths < 45 km), which is significantly deeper compared to the Neoproterozoic Fuchuan mantle-hosted granitoids (< 12 - 15 km). Therefore, we suggest that during the Neoproterozoic era, the transport depth of sediment-derived melts from subducting slabs into the mantle was substantially shallower compared to modern subduction systems and this was likely linked to elevated mantle potential temperatures relative to present-day Earth (van Keken et al., 2018).

Some research reveals that mantle potential temperatures have decreased to below 80-100 ℃ relative to modern Earth since the Neoproterozoic. This suggests the establishment of a globally connected deep subduction system under modern-style plate tectonic paradigm characterized by enhanced orogenic activity, increased sediment flux to subduction zones and high P/T metamorphic records with low thermal gradients (<350°C/GPa) (Campbell and Squire, 2010; Cawood et al., 2024; Sobolev and Brown, 2019; Stern, 2025; Yao et al., 2021). This tectonic shift facilitated massive sediment recycling into the mantle through subduction processes (Sobolev and Brown, 2019; Wang et al., 2020; Zhao et al., 2022; Zheng and Zhao, 2020), promoting the generation of mantle-hosted S-type granitoids, associated arc magmatism (e.g., boninitic melts) and abundant SSZ-type ophiolites along the margin of Rodinia (Huang et al., 2021; Tang et al., 2021). The Fuchuan mantle-hosted granitoids, representing the earliest known mantle-hosted S-type granitoids formed at shallow depths during oceanic slab subduction, may well mark the initial manifestation of modern-style plate tectonics under elevated mantle potential temperatures compared to present-day conditions.

A range of geochemical evidence indicates the recycling of supracrustal rocks (e.g., altered oceanic crust and pelagic sediments) into the mantle during the Archean. This evidence includes: a) the heavy Si-O isotopic signatures detected in Archean zircons from the North China, Slave, Siberia, Antarctica, Greenland, and Australia cratons

(Guitreau et al., 2022; Zhang et al., 2023; Wang et al., 2022); b) atmospheric sulfur isotope anomalies identified in Eoarchean meta-mafic rocks from the Innuksuac Complex, Canada (Caro et al., 2025); c) late Archean sulfide inclusions within lithospheric diamonds of eclogitic paragenesis (Farquhar et al., 2002; Smit et al., 2019). However, the Archean mantle was approximately 300 K hotter than present-day ambient mantle, and such elevated temperatures would have significantly influenced the feasibility and mode of subduction processes (Fischer and Gerya, 2016). Consequently, widely invoked models for early plate tectonics involves shallow and flat subduction (Foley et al., 2003; Johnson et al., 2014; Lu et al., 2024a, Wang et al., 2022a) or sagduction process triggered by mantle plumes (Yu et al., 2022). These processes would have inhibited deep subduction under low thermal gradients. This is further supported by the absence of Archean ophiolites and high P/T metamorphic records.

The emergence of ca. 2.2-1.8 Ga ophiolite suites (e.g., the Flin Flon ophiolite and Jormua ophiolites; Peltonen et al., 1996; Scott et al., 1992) and contemporaneous high P/T blueschists/eclogites formed under low thermal gradients (e.g., eclogite xenoliths found in Paleoproterozoic carbonatites within the North China Craton; Brown and Johnson, 2019; Weller and St-Onge, 2017; Xu et al., 2018), may indicate a short-lived period of globally connected deep subduction during Paleoproterozoic mantle cooling. The recycling of surficial crustal materials at this time, including sediments, is evidenced by increasing alkaline content and Nb/Ta ratios in igneous rocks, elevated mantle oxygen fugacity, and signals from the deep carbon cycle (Liu et al., 2019; 2023; 2025, 2025a; Moreira et al., 2023). However, this transient phase of global deep subduction may have ceased following the assembly of the Nuna/Columbia supercontinent. Because mantle temperature likely rose again from 2.2 to 1.8 Ga with enhanced continental insulation effects associated with supercontinent consolidation (Lu et al., 2024), leading to an extended period of "single-lid" tectonics throughout Earth's middle age (Cawood et al., 2014; Huang et al., 2025; Stern, 2025; Tang et al., 2021; Zhang et al., 2025).

5.5. Implication for the generation of S-type granitoids

S-type granitoids are largely derived from partial melting of pre-existing metasedimentary/other supracrustal materials (Wang et al., 2013b, 2023). They occur across a range of geodynamic settings including ocean-continent subduction accretionary orogens and continent-continent collisional orogens, as well as continental rifts (Collins and Richards, 2008; Zhu et al., 2023), and thus represent intracrustal fractionation of crustal components via anataxis (Ackerson et al., 2018; Kemp et al., 2007; Schaen et al., 2021). The discovery of mantle-hosted S-type granitoids points to subduction initiation as a potential mechanism for the recycling of sediments at the mantle depth. In addition, the sharp contact observed between the felsic intrusions and mantle peridotite in the Fuchuan Ophiolite (Fig. 2a-b) signifies rapid solidification within a cold and shallow mantle wedge corner. This implies a steep thermal gradient during subduction initiation created a narrow and transient hot zone within the corner, resulting in the proximal emplacement of granitic melts and thereby precluding any long-distance migration. This phenomenon is consistent with the observation of these granitoids in the Samail Ophiolite (Rioux et al., 2021; Rollinson, 2015), suggesting that sediment-derived melts can be preserved within the mantle wedge corner, and thus they hold the potential to significantly contribute to the heterogeneity of the mantle.

6. Conclusions

A suite of mantle-hosted S-type granitoids within the Neoproterozoic Fuchuan supra-subduction zone ophiolite in South China has been newly identified in this study. These mantle-hosted granitoids emplaced at ca. 837 - 846 Ma and are coeval with the subduction-related mafic-ultramafic rocks (848 - 820 Ma) within the Fuchuan Ophiolite, implying the former's emplacement during oceanic slab subduction rather than late obduction. Geochemical analyses and pseudosection modeling collectively reveal that these felsic intrusions formed during subduction initiation and so are a crucial proxy for subduction initiation. In contrast to the generation depth of the Phanerzoic mantle-hosted S-type granitoids, Neoproterozoic sediment-derived melt transport from subducting slabs occurred at substantially shallower depths, hinting that the Neoproterozoic era likely witnesses the re-operation of modern-style plate tectonic paradigm after ceasing of Paleoproterozoic deep subduction.

CRediT authorship contribution statement

Sifang Huang: Validation, Software, Resources, Methodology, Formal analysis, Data curation, Methodology, Funding acquisition, Conceptualization, Writing – original draft, review and editing. **Wei Wang:** Writing – review & editing, Supervision,

Investigation, Conceptualization, Visualization, Funding acquisition. **Andrew C. Kerr:** Writing – review & editing, Visualization. **Peter A. Cawood:** Writing – review & editing, Visualization, Conceptualization, Funding acquisition. **Guimei Lu:** Writing – review & editing, Software.

Declaration of competing interest

The authors declare that they have no competing financial interests or personal relationships that could have appeared to influence the work reported in this paper.

Acknowledgements

We thank the editors for their effective handling of the manuscript and additional comments. We are also grateful to two anonymous reviewers whose insightful and constructive reviews greatly improved this manuscript. This work was supported by the National Natural Scientific Foundation of China (42272228), the Natural Science Foundation of Henan Province (242300421663), the Natural Science Foundation of Hubei Province (2025AFA033), the Shangqiu Normal University Doctor Research Start-up Fund and the Australian Research Council (FL160100168).

Data availability

Data are available at https://doi.org/10.6084/m9.figshare.30175099.

References

Ackerson, M. R., Mysen, B. O., Tailby, N. D., Watson, E. B., 2018. Low-temperature crystallization of granites and the implications for crustal magmatism. Nature 559, 94-97. https://doi.org/10.1038/s41586-018-0264-2.

Angelo, T. V., Spencer, C. J., Cavosie, A. J., Thomas, R., Li, H. Y., 2023. Petrogenesis of Mantle-Hosted Granitoids from the Samail Ophiolite. J. Petrol. 64, egad021. https://doi.org/10.1093/petrology/egad021.

Bai, W. J., Gan, Q. G., Yang, J. S., Xing, F. M., Xu, X., 1989. Discovery of Well-reserved Ophiolite and Its Basical Characters in Southeastern Margin of the Jiangnan Ancient Continent. Acta Petrol. Mineral. 5, 289-299. (in Chinese with English Abstract)

Behn, M. D., Kelemen, P. B., Hirth, G., Hacker, B. R., Massonne, H. J., 2011. Diapirs as the source of the sediment signature in arc lavas. Nat. Geosci. 4, 641-646. https://doi.org/10.1038/ngeo1214.

Bell, E. A., Boehnke, P., Harrison, T. M., 2016. Recovering the primary geochemistry of Jack Hills zircons through quantitative estimates of chemical alteration. Geochim. Cosmochim. Acta 191, 187-202. https://doi.org/10.1016/j.gca.2016.07.016.

Boehnke, Patrick., Watson, E. B., Trail, D., Harrison, T. M., Schmitt, A. K., 2013. Zircon saturation re-revisited. Chem. Geol. 351, 324-334. https://doi.org/10.1016/j.chemgeo.2013.05.028.

Brown, M., Johnson, T., 2019. Metamorphism and the evolution of subduction on Earth. Am. Miner. 104, 1065-1082. https://doi.org/10.2138/am-2019-6956.

Burnham, A. D., Berry, A. J., 2017. Formation of Hadean granites by melting of igneous crust. Nat. Geosci. 10, 457-461. https://doi.org/10.1038/ngeo2942.

Campbell, I. H, Squire, R. J., 2010. The mountains that triggered the Late Neoproterozoic increase in oxygen: The Second Great Oxidation Event. Geochim. Cosmochim. Acta 74, 4187-4206. https://doi.org/10.1016/j.gca.2010.04.064.

Caro, G., Grocolas, T., Bourgeois, P., Bouilhol, P., Mojzsis, S.J., Paris, G., 2025. Early Archaean onset of volatile cycling at subduction zones. Nat. Geosci. 18, 436-442. https://doi.org/10.1038/s41561-025-01677-5.

Cawood, P. A., Merdith, A. S., Murphy, J. B., 2024. Syn-emplacement ophiolites and relationship to supercontinent cycle. Earth Planet. Sci. Lett. 641, 118810. https://doi.org/10.1016/j.epsl.2024.118810.

Cawood, P. A., Hawkesworth, C. J., 2014. Earth's middle age. Geology 42, 503-506. https://doi.org/10.1130/G35402.1.

Chen, F., Zhu, X. Y., Wang, W., Wang, F., Trung, H. P., Siebel, W., 2009. Single-grain detrital muscovite Rb-Sr isotopic composition as an indicator of provenance for the Carboniferous sedimentary rocks in northern Dabie, China. Geochem. J. 43, 257-273. https://doi.org/10.2343/geochemj.1.0023.

Chen, J., Jahn, B. M., 1998. Crustal evolution of southeastern China: Nd and Sr isotopic evidence. Tectonophysics 284, 101-133. https://doi.org/10.1016/S0040-1951(97)00186-8.

Cheng, H., 1993. Geochemsitry of Proterozoic Island-arc Volcanic Rocks in Northwest Zhejiang. Geochimica 1, 18-27. https://doi.org/10.19700/j.0379-1726.1993.01.003. (in Chinese with English Abstract)

Collins, W. J., Richards, S. W., 2008. Geodynamic significance of S-type granites in circum-Pacific orogens. Geology 36, 559-562. https://doi.org/10.1130/G24658A.1.

Cox, J., Searle, M., Pedersen, R., 1999. The petrogenesis of leucogranitic dykes intruding the northern Semail ophiolite, United Arab Emirates: field relationships, geochemistry and Sr/Nd isotope systematics. Contrib. Mineral. Petrol. 137, 267-287. https://doi.org/10.1007/s004100050550.

Çörtük, R. M., Çelik, Ö. F., Özkan, M., Davies, J., Marzoli, A., 2024. Timing of the subduction initiation and ophiolite emplacement of the inner Tauride Ocean: Insight from the Pınarbaşı ophiolite in Central Türkiye. Lithos 488-489, 107833. https://doi.org/10.1016/j.lithos.2024.107833.

Cruz-Uribe, A. M., Marschall, H. R., Gaetani, G. A., Roux, V. L., 2018. Generation of alkaline magmas in subduction zones by partial melting of mélange diapirs-An experimental study. Geology 46, 343-346. https://doi.org/10.1130/G39956.1.

de Kock, M. O., Malatji, I., Wabo, H., Mukhopadhyay, J., Banerjee, A., Mare, L. P., 2024. High-latitude platform carbonate deposition constitutes a climate conundrum at the terminal Mesoproterozoic. Nat. Commun. 15, 2024. https://doi.org/10.1038/s41467-024-46390-w

Ding, B. H., Shi, R. D., Zhi, X. C., Zheng, L., Chen, L., 2008. Neoproterozoic (~850Ma) subduction in the Jiangnan orogen: evidence from the SHRIMP U-Pb dating of the SSZ-type ophiolite in southern Anhui Province. Acta Petrol. Mineral. 27, 375-388. https://doi.org/10.3969/j.issn.1000-6524.2008.05.001 (in Chinese with English Abstract)

Farquhar, J., Wing, B.A., McKeegan, K.D., Harris, J.W., Cartigny, P., Thiemens, M.H., 2002. Mass-Independent Sulfur of Inclusions in Diamond and Sulfur Recycling on Early Earth. Science 298, 2369-2372. https://doi.org/10.1126/science.1078617.

Fischer, R., Gerya, T., 2016. Regimes of subduction and lithospheric dynamics in the Precambrian: 3D thermomechanical modelling. Gondwana Res. 37, 53-70. https://doi.org/10.1016/j.gr.2016.06.002.

Foley, S. F., Buhre, S., Jacob, D. E., 2003. Evolution of the Archaean crust by delamination and shallow subduction. Nature 421, 249-252. https://doi.org/10.1038/nature01319.

Gao, J., Klemd, R., Long, L., Xiong, X., Qian, Q., 2009. Adakitic signature formed by fractional crystallization: An interpretation for the Neo-Proterozoic meta-plagiogranites of the NE Jiangxi ophiolitic mélange belt, South China. Lithos 110, 277-293. https://doi.org/10.1016/j.lithos.2009.01.009.

Gerya, T. V., 2011. Intra-oceanic Subduction Zones, in: Brown, D., Ryan, P.D., Arc-Continent Collision. Springer-Verlag, Berlin, pp. 23-51. https://doi.org/10.1007/978-3-540-88558-0_2.

Guillot, S., Le Fort, P., 1995. Geochemical constraints on the bimodal origin of High Himalayan leucogranites. Lithos 35, 221-234. https://doi.org/10.1016/0024-4937(94)00052-4.

Guitreau, M., Gannoun, A., Deng, Z., Chaussidon, M., Moynier, F., Barbarin, B., Marin-Carbonne, J., 2022. Stable isotope geochemistry of silicon in granitoid zircon. Geochim. Cosmochim. Acta 316, 273-294. https://doi.org/10.1016/j.gca.2021.09.029.

Guo, L. Z., Shi, Y. S., Ma, R. S., Ye, S. F., Lu, H. F., 1984. Tectonostratgraphic Terranes of Southeast China. J. Nanjing Univ. (Nat. Sci.) 20, 732-739. (in Chinese with English Abstract)

Guo, Z., Wilson, M., 2012. The Himalayan leucogranites: Constraints on the nature of their crustal source region and geodynamic setting. Gondwana Res. 22, 360-376. https://doi.org/10.1016/j.gr.2011.07.027.

Haase, K. M., Freund, S., Koepke, J., Hauff, F., Erdmann, M., 2015. Melts of sediments in the mantle wedge of the Oman ophiolite. Geology 43, 275-278. https://doi.org/10.1130/G36451.1.

Hall, C. E., Gurnis, M., Sdrolias, M., Lavier, L. L., Müller, R. D., 2003. Catastrophic initiation of subduction following forced convergence across fracture zones. Earth Planet. Sci. Lett. 212, 15-30.

https://doi.org/10.1016/S0012-821X(03)00242-5.
Hermann, J., Rubatto, D., 2009. Accessory phase control on the trace element signature of sediment melts in subduction zones. Chem. Geol. 265, 512-526. https://doi.org/10.1016/j.chemgeo.2009.05.018.
Holland, T., Powell, R., 2011. An improved and extended internally consistent thermodynamic dataset for phases of petrological interest, involving a new equation of state for solids. J. Metamorph. Geol. 29, 333-383. https://doi.org/10.1111/j.1525-1314.2010.00923.x.
Huang, S. F., Lu, G. M., Yu, F., Zhu, X., He, Z., Li, R., Zhang, M. D., Li, Q. W., Wang, W., 2025. Neoproterozoic backarc S-type granite in the Jiangnan fold belt, South China: Implication for initiation of modern-style plate tectonics. Geol. Soc. Am. Bull. https://doi.org/10.1130/B38197.1. inpress.
Huang, S. F., Wang, W., Kerr, A. C., Zhao, J. H., Xiong, Q., Wang, J., 2021. The Fuchuan Ophiolite in South China: Evidence for Modern‐Style Plate Tectonics During Rodinia Breakup. Geochem. Geophys. Geosyst. 22, e2021GC010137. https://doi.org/10.1029/2021GC010137.
Huang, S. F., Wang, W., Pandit, M. K., Zhao, J. H., Lu, G. M., Xue, E. K., 2019. Neoproterozoic S-type granites in the western Jiangnan Orogenic Belt, South China: Implications for petrogenesis and geodynamic significance. Lithos 342-343, 45-58. https://doi.org/10.1016/j.lithos.2019.05.016.
Ishikawa, T., Fujisawa, S., Nagaishi, K., Masuda, T., 2005. Trace element characteristics of the fluid liberated from amphibolite-facies slab: Inference from the metamorphic sole beneath the Oman ophiolite and implication for boninite genesis. Earth Planet. Sci. Lett. 240, 355-377. https://doi.org/10.1016/j.epsl.2005.09.049.
Jackson, S. E., Pearson, N. J., Griffin, W. L., Belousova, E. A., 2004. The application of laser ablation-inductively coupled plasma-mass spectrometry to in situ U-Pb zircon geochronology. Chem. Geol. 211, 47-69. https://doi.org/10.1016/j.chemgeo.2004.06.017.
Johnson, M. C., Plank, T., 1999. Dehydration and melting experiments constrain the fate of subducted sediments. Geochem. Geophys. Geosyst. 1, 1007. https://doi.org/10.1029/1999GC000014.
Johnson, T. E., Brown, M., Kaus, B. J. P., VanTongeren, J. A., 2014. Delamination and recycling of Archaean crust caused by gravitational instabilities. Nat. Geosci. 7, 47-52. https://doi.org/10.1038/ngeo2019.
Kemp, A. I., Hawkesworth, C. J., Foster, G. L., Paterson, B. A., Woodhead, J. D., Hergt, J. M., Gray, C. M., Whitehouse, M. J., 2007. Magmatic and crustal differentiation history of granitic rocks from Hf-O isotopes in zircon. Science 315, 980-983. https://doi.org/10.1126/science.1136154.
Kessel, R., Schmidt, M. W., Ulmer, P., Pettke, T., 2005. Trace element signature of subduction-zone fluids, melts and supercritical liquids at 120-180 km depth. Nature 439, 724-727. https://doi.org/10.1038/nature03971.
Klaver, M., Yogodzinski, G., Albert, C., Camejo-Harry, M., Elburg, M., Hoernle, K., Macpherson, C., Nowell, G., Rushmer, T., Williams, H., Millet, M. A., 2024. Widespread slab melting in modern subduction zones. Earth Planet. Sci. Lett. 626, 118544. https://doi.org/10.1016/j.epsl.2023.118544.
Klein, B. Z., Behn, M. D., 2021. On the Evolution and Fate of Sediment Diapirs in Subduction Zones. Geochem. Geophys. Geosyst. 22, e2021GC009873. https://doi.org/10.1029/2021GC009873.
Li, H., Hermann, J., Zhang, L., 2022. Melting of subducted slab dictates trace element recycling in global arcs. Sci. Adv. 8, eabh2166. https://doi.org/10.1126/sciadv.abh2166.
Li, H., Wang, M., Zeng, X. W., Luo, A. B., Zhang, B. C., Shen, D., 2022a. Partial melting caused by subduction of young, hot oceanic crust in shallow high-temperature and low-pressure environments: Indications from Middle and Late Jurassic oceanic plagiogranite in Shiquanhe, Central Tibet. Lithos 420-421, 106698. https://doi.org/10.1016/j.lithos.2022.106698.
Li, H. Y., Li, X., Ryan, J. G., Zhang, C., Xu, Y.G., 2022b. Boron isotopes in boninites document rapid changes in slab inputs during subduction initiation. Nat. Commun. 13, 993. https://doi.org/10.1038/s41467-022-28637-6
Li, Q. W., Zhao, J. H., 2020. Amalgamation between the Yangtze and Cathaysia Blocks in South China: Evidence from the ophiolite geochemistry. Precambrian Res. 350, 105893. https://doi.org/10.1016/j.precamres.2020.105893.
Li, W. X., Li, X. H., 2003. Adakitic granites within the NE Jiangxi ophiolites, South China: geochemical and Nd isotopic evidence. Precambrian Res. 122, 29-44. https://doi.org/10.1016/S0301-9268(02)00206-1.
Li, W. X., Li, X. H., Li, Z. X., Lou, F. S., 2008. Obduction-type granites within the NE Jiangxi Ophiolite: Implications for the final amalgamation between the Yangtze and Cathaysia Blocks. Gondwana Res. 13, 288-301. https://doi.org/10.1016/j.gr.2007.12.010.
Li, X. H., Li, Z. X., Ge, W., Zhou, H., Li, W., Liu, Y., Wingate, M. T. D., 2003. Neoproterozoic granitoids in South China: crustal melting above a mantle plume at ca. 825 Ma? Precambrian Res. 122, 45-83.

https://doi.org/10.1016/S0301-9268(02)00207-3.

Li, X. H., Long, W. G., Li, Q. L., Yu, L., Tao, H., 2010. Penglai Zircon Megacrysts: A Potential New Working Reference Material for Microbeam Determination of Hf-O Isotopes and U-Pb Age. Geostand. Geoanal. Res. 34, 117-134. https://doi.org/10.1111/j.1751-908X.2010.00036.x.

Li, Y., Zhang, Z., Santosh, M., Wang, G., Wang, J., Dong, P., Li, H., Kong, W., 2023. Continental crustal growth and differentiation in intraoceanic arcs: Insights from plagiogranites in the forearc ophiolite of the southeastern Central Asian Orogenic Belt, China. Lithos 454-455, 107289. https://doi.org/10.1016/j.lithos.2023.107289.

Liu, D., Xu, C., Brenna, M., Liu, X., Li, Q., Wei, C., 2025a. Paleoproterozoic deep carbon cycle recorded in carbonatites. Precambrian Res. 417, 107669. https://doi.org/10.1016/j.precamres.2024.107669.

Liu, H., Sun, W. D., Zartman, R., Tang, M., 2019. Continuous plate subduction marked by the rise of alkali magmatism 2.1 billion years ago. Nat. Commun. 10, 3408. https://doi.org/10.1038/s41467-019-11329-z.

Liu, H., Wang, Y., Deng, J., Zhang, Y., Chen, Q., Liao, R., Sun, W. D., 2023. Modern-style arc magmatism since ca. 2.2 billion years ago revealed by Nb/Ta-Dy/Yb systematics in igneous rocks. Chem. Geol. 638, 121710. https://doi.org/10.1016/j.chemgeo.2023.121710.

Liu, Y., Gao, S., Hu, Z., Gao, C., Zong, K., Wang, D., 2010. Continental and Oceanic Crust Recycling-induced Melt-Peridotite Interactions in the Trans-North China Orogen: U-Pb Dating, Hf Isotopes and Trace Elements in Zircons from Mantle Xenoliths. J. Petrol. 51, 537-571. https://doi.org/10.1093/petrology/egp082.

Lu, G. M., Xu, Y. G., Wang, W., Spencer, C. J., Roberts, N. M. W., Condie, K. C., 2024. Diverse source materials contributed to a secular increase in $\delta^{18}O$ for the Paleo-Mesoproterozoic A_2-type granites. Earth Planet. Sci. Lett. 642, 118885. https://doi.org/10.1016/j.epsl.2024.118885.

Lu, G. M., Xu, Y. G., Wang, W., Spencer, C. J., Huang, G., Roberts, N. M., 2024a. Continental crust rejuvenation across the Paleo-Mesoarchean transition resulted from elevated mantle geotherms. Geophys. Res. Lett. 51, e2024GL108715. https://doi.org/10.1029/2024GL108715.

Moreira, H., Storey, C., Bruand, E., Darling, J., Fowler, M., Cotte, M., Villalobos-Portillo, E. E., Parat, F., Seixas, L., Philippot, P., Dhuime, B., 2023. Sub-arc mantle fugacity shifted by sediment recycling across the Great Oxidation Event. Nat. Geosci. 16, 922-927. https://doi.org/10.1038/s41561-023-01258-4.

Peltonen, P., Kontinen, A., Huhma, H., 1996. Petrology and Geochemistry of Metabasalts from the 1.95 Ga Jormua Ophiolite, Northeastern Finland. J. Petrol. 37, 1359-1383. https://doi.org/10.1093/petrology/37.6.1359.

Plank, T., Langmuir, C. H., 1998. The chemical composition of subducting sediment and its consequences for the crust and mantle. Chem. Geol. 145, 325-394. https://doi.org/10.1016/S0009-2541(97)00150-2.

Rapp, R. P., Watson, E. B., Miller, C. F., 1991. Partial melting of amphibolite/eclogite and the origin of Archean trondhjemites and tonalites. Precambrian Res. 51, 1-25. https://doi.org/10.1016/0301-9268(91)90092-O.

Rebaza, A. M., Mallik, A., Cooperdock, E. H. G., Holman, B. I., 2024. The fate of ultramafic-rich mélanges in cold to hot subduction zones: Implications for diapirism (or not) and chemical geodynamics. Earth Planet. Sci. Lett. 647, 119020. https://doi.org/10.1016/j.epsl.2024.119020.

Retallack, G. J., 2013. Ediacaran life on land. Nature 493, 89-92. https://doi.org/10.1038/nature11777.

Rioux, M., Benoit, M., Amri, I., Ceuleneer, G., Garber, J. M., Searle, M., Leal, K., 2021. The Origin of Felsic Intrusions Within the Mantle Section of the Samail Ophiolite: Geochemical Evidence for Three Distinct Mixing and Fractionation Trends. J. Geophys. Res.-Solid Earth 126, e2020JB020760. https://doi.org/10.1029/2020JB020760.

Rollinson, H., 2015. Slab and sediment melting during subduction initiation: granitoid dykes from the mantle section of the Oman ophiolite. Contrib. Mineral. Petrol. 170, 32. https://doi.org/10.1007/s00410-015-1177-9.

Rushmer, T., 1991. Partial melting of two amphibolites: contrasting experimental results under fluid-absent conditions. Contrib. Mineral. Petrol. 107, 41-59. https://doi.org/10.1007/BF00311184.

Schaen, A. J., Schoene, B., Dufek, J., Singer, B. S., Eddy, M. P., Jicha, B. R., Cottle, J. M., 2021. Transient rhyolite melt extraction to produce a shallow granitic pluton. Sci. Adv. 7, eabf0604. https://doi.org/10.1126/sciadv.abf0604

Scott, D. J., Helmstaedt, H., Bickle, M. J., 1992. Purtuniq ophiolite, Cape Smith belt, northern Quebec, Canada: A reconstructed section of Early Proterozoic oceanic crust. Geology 20, 173-176. https://doi.org/10.1130/0091-7613(1992)020<0173:POCSBN>2.3.CO;2.

Şen, C., Dunn, T., 1994. Dehydration melting of a basaltic composition amphibolite at 1.5 and 2.0 GPa: implications for the origin of adakites. Contrib. Mineral. Petrol. 117, 394-409.

https://doi.org/10.1007/BF00307273.

Shen, W. Z., Zhu, J. C., Liu, C. S., Xu, S. J., Ling, H. F., 1993. Sm-Nd isotopic study of basement metamorphic rocks in South China and its constraint on material sources of granitoids. Acta Petrol. Sin. 9, 115-124. (in Chinese with English Abstract)

Shu, L., Wang, J., Yao, J., 2019. Tectonic evolution of the eastern Jiangnan region, South China: New findings and implications on the assembly of the Rodinia supercontinent. Precambrian Res. 322, 42-65. https://doi.org/10.1016/j.precamres.2018.12.007.

Shu, L. S., Zhou, G. Q., Shi, Y. S., Yin, J., 1994. Study of the high metamorphic blueschist and its late Proterozoic age in the eastern Jiangnan Belt. Chin. Sci. Bull. 39, 1200-1204. https://doi.org/10.1360/csb1993-38-20-1879.

Shui, T., Xu, B. T., Liang, R. H., Qiu, Y. S., 1986. The ancient land connection belt of Jiangshan – Shaoxing. Chin. Sci. Bull. 31, 444-448. https://doi.org/10.1360/csb1986-31-6-444. (in Chinese).

Sláma, J., Košler, J., Condon, D. J., Crowley, J. L., Gerdes, A., Hanchar, J. M., Horstwood, M. S. A., Morris, G. A., Nasdala, L., Norberg, N., Schaltegger, U., Schoene, B., Tubrett, M. N., Whitehouse, M. J., 2008. Plešovice zircon - A new natural reference material for U-Pb and Hf isotopic microanalysis. Chem. Geol. 249, 1-35. https://doi.org/10.1016/j.chemgeo.2007.11.005.

Smit, K. V., Shirey, S. B., Hauri, E. H., Stern, R. A., 2019. Sulfur isotopes in diamonds reveal differences in continent construction. Science 364, 383-385. https://doi.org/10.1126/science.aaw9548.

Sobolev, S. V., Brown, M., 2019. Surface erosion events controlled the evolution of plate tectonics on Earth. Nature 570, 52-57. https://doi.org/10.1038/s41586-019-1258-4.

Spencer, C. J., Cavosie, A. J., Raub, T. D., Rollinson, H., Evans, N. J., 2017. Evidence for melting mud in Earth's mantle from extreme oxygen isotope signatures in zircon. Geology 45, 975-978. https://doi.org/10.1130/G39402.1.

Stern, R. J., 2002. Subduction zones. Rev. Geophys. 40, 1012. https://doi.org/10.1029/2001RG000108.

Stern, R. J., 2025. A reinterpretation of the past 2.5 billion years of Earth's tectonic history: Two episodes each of plate and single-lid tectonics. Geol. Soc. Am. Bull. 137, 2079-2100. https://doi.org/10.1130/B37966.1.

Sun, Z. M., Wang, X. L., Zhang, F. F., Xie, H. Q., Zhao, K., Li, J. Y., 2020. Diversity of Felsic Rocks in Oceanic Crust: Implications From the Neoproterozoic Plagiogranites Within the Northeast Jiangxi Ophiolite, Southern China. J. Geophys. Res.-Solid Earth 125, e2019JB017414. https://doi.org/10.1029/2019JB017414.

Sylvester, P. J., 1998. Post-collisional strongly peraluminous granites. Lithos 45, 29-44. https://doi.org/10.1016/S0024-4937(98)00024-3.

Tang, M., Chu, X., Hao, J., Shen, B., 2021. Orogenic quiescence in Earth's middle age. Science 371, 728-731. https://doi.org/10.1126/science.abf1876.

Tang, M., Wang, X.L., Shu, X.J., Wang, D., Yang, T., Gopon, P., 2014, Hafnium isotopic heterogeneity in zircons from granitic rocks: Geochemical evaluation and modeling of "zircon effect" in crustal anatexis. Earth Planet. Sci. Lett. 389, 188-199, https://doi .org /10 .1016 /j .epsl .2013 .12 .036.

Tommasini, S., Avanzinelli, R., Conticelli, S., 2011. The Th/La and Sm/La conundrum of the Tethyan realm lamproites. Earth Planet. Sci. Lett. 301, 469-478. https://doi.org/10.1016/j.epsl.2010.11.023.

Valley, J. W., Bindeman, I. N., Peck, W. H., 2003. Empirical calibration of oxygen isotope fractionation in zircon. Geochim. Cosmochim. Acta 67, 3257-3266. https://doi.org/10.1016/S0016-7037(03)00090-5.

van Keken, P. E., Wada, I., Abers, G. A., Hacker, B. R., Wang, K., 2018. Mafic High-Pressure Rocks Are Preferentially Exhumed From Warm Subduction Settings. Geochem. Geophys. Geosyst. 19, 2934-2961. https://doi.org/10.1029/2018GC007624.

Vermeesch, P., 2018. IsoplotR: A free and open toolbox for geochronology. Geosci. Front. 9, 1479-1493. https://doi.org/10.1016/j.gsf.2018.04.001.

Wang, J., Gong, Y., Hu, X., Shi, H., Jiang, K., 2023. Petrogenesis of granitoids in the southern Anhui Province, China: Implications for the Neoproterozoic tectonic evolution of the eastern Jiangnan orogenic belt. Precambrian Res. 397, 107194. https://doi.org/10.1016/j.precamres.2023.107194.

Wang, W., Zhou, M. F., Yan, D. P., Li, L., Malpas, J., 2013a. Detrital zircon record of Neoproterozoic active-margin sedimentation in the eastern Jiangnan Orogen, South China. Precambrian Res. 235, 1-19. https://doi.org/10.1016/j.precamres.2013.05.013.

Wang, W., Zhou, M. F., Zhao, J. H., Pandit, M. K., Zheng, J. P., Liu, Z. R., 2016. Neoproterozoic active continental margin in the southeastern Yangtze Block of South China: Evidence from the ca. 830-810 Ma sedimentary strata. Sediment. Geol. 342, 254-267. https://doi.org/10.1016/j.sedgeo.2016.07.006.

Wang, W., Cawood, P. A., Spencer, C., Pandit, M. K, Zhao, J. H., Xia, X. P., Zheng, J. P., Lu G. M., 2022a. Global-scale emergence of continental crust during the Mesoarchean and early Neoarchean, Geology 50, 184-188. https://doi.org/10.1130/G49418.1.

Wang, X. L., Liu, F., Li, J., Wang, D., 2020. The progressive onset and evolution of Precambrian subduction and plate tectonics. Sci. China-Earth Sci. 63, 2068-2086. https://doi.org/10.1007/s11430-020-9698-0.

Wang, X. L., Zhou, J. C., Wan, Y. S., Kitajima, K., Wang, D., Bonamici, C., Qiu, J. S., Sun, T., 2013b. Magmatic evolution and crustal recycling for Neoproterozoic strongly peraluminous granitoids from southern China: Hf and O isotopes in zircon. Earth Planet. Sci. Lett. 366, 71-82. https://doi.org/10.1016/j.epsl.2013.02.011.

Wang, X. L, Tang, M., Moyen, J., Wang, D., Kröner, A., Hawkesworth, C., Xia, X., Xie, H., Anhaeusser, C., Hofmann, A., Li, J., Li, L., 2022. The onset of deep recycling of supracrustal materials at the Paleo-Mesoarchean boundary. Natl. Sci. Rev. 9, nwab136. https://doi.org/10.1093/nsr/nwab136.

Watson, E.B., Harrison, T.M., 2005. Zircon Thermometer Reveals Minimum Melting Conditions on Earliest Earth. Science 308, 841–844. https://doi.org/10.1126/ science.1110873.

Weller, O. M., St-Onge, M. R. 2017., Record of modern-style plate tectonics in the Palaeoproterozoic Trans-Hudson orogen. Nat. Geosci. 10, 305-311. https://doi.org/10.1038/ngeo2904.

White, R. W., Powell, R., Holland, T. J. B., Johnson, T. E., Green, E., 2014. New mineral activity-composition relations for thermodynamic calculations in metapelitic systems. J. Metamorph. Geol. 32, 261-286. https://doi.org/10.1111/jmg.12071.

Whitehead, J., Dunning, G.R., Spray, J.G., 2000. U-Pb geochronology and origin of granitoid rocks in the Thetford Mines ophiolite, Canadian Appalachians. Geol. Soc. Am. Bull. 112, 915-928. https://doi.org/10.1130/0016-7606(2000)112<915:UGAOOG>2.0.CO;2.

Wu, R. X., Zheng, Y. F., Wu, Y. B., Zhao, Z. F., Zhang, S. B., Liu, X. M., Wu, F. Y., 2006. Reworking of juvenile crust: element and isotope evidence from Neoproterozoic granodiorite in South China. Precambrian Res. 146, 179-212. https://doi.org/10.1016/j.precamres.2006.01.012.

Xiang, H., Connolly, J. A. D., 2022. GeoPS: An interactive visual computing tool for thermodynamic modelling of phase equilibria. J. Metamorph. Geol. 40, 243-255. https://doi.org/10.1111/jmg.12626.

Xu, C., Kynický, J., Song, W., Tao, R., Lü, Z., Li, Y., Yang, Y., Pohanka, M., Galiova, M. V., Zhang, L., Fei, Y., 2018. Cold deep subduction recorded by remnants of a Paleoproterozoic carbonated slab. Nat. Commun. 9, 2790. https://doi.org/10.1038/s41467-018-05140-5.

Xu, X., Xue, D., Li, Y., Hu, P., Chen, N., 2014. Neoproterozoic sequences along the Dexing-Huangshan fault zone in the eastern Jiangnan orogen, South China: Geochronological and geochemical constrains. Gondwana Res. 25, 368-382. https://doi.org/10.1016/j.gr.2013.03.020.

Xu, X. S., Zhou, X. M., 1989. Rock Inclusion within Precambrian Granitoids in South Anhui Province. Mineral. Petrol. 11, 24-28. https://doi.org/:10.19719/j.cnki.1001-6872.1991.01.005.

Yang, Q., Xia, X., Zhang, W., Zhang, Y., Xiong, B., Xu, Y., Wang, Q., Wei, G., 2018. An evaluation of precision and accuracy of SIMS oxygen isotope analysis. Solid Earth Sci. 3, 81-86. https://doi.org/10.1016/j.sesci.2018.05.001.

Yao, J., Cawood, P. A., Shu, L. S., Zhao, G. C., 2019. Jiangnan Orogen, South China: A ~970-820 Ma Rodinia margin accretionary belt. Earth-Sci. Rev. 196, 102872. https://doi.org/10.1016/j.earscirev.2019.05.016.

Yao, J., Cawood, P. A., Zhao, G., Han, Y., Xia, X., Liu, Q., Wang, P., 2021. Mariana-type ophiolites constrain the establishment of modern plate tectonic regime during Gondwana assembly. Nat. Commun. 12, 4189. https://doi.org/10.1038/s41467-021-24422-z.

Yin, C., Lin, S., Davis, D. W., Xing, G., Davis, W. J., Cheng, G., Xiao, W., Li, L., 2013. Tectonic evolution of the southeastern margin of the Yangtze Block: Constraints from SHRIMP U-Pb and LA-ICP-MS Hf isotopic studies of zircon from the eastern Jiangnan Orogenic Belt and implications for the tectonic interpretation of South China. Precambrian Res. 236, 145-156. https://doi.org/10.1016/j.precamres.2013.07.022.

Yu, C., Yang, T., Zhang, J., Zhao, G., Cawood, P.A., Yin, C., Qian, J., Gao, P., Zhao, C., 2022. Coexisting diverse P-T-t paths during Neoarchean Sagduction: Insights from numerical modeling and applications to the eastern North China Craton. Earth Planet. Sci. Lett. 586, 117529. https://doi.org/10.1016/j.epsl.2022.117529.

Zhang, C. L., Santosh, M., Zou, H. B., Li, H. K., Huang, W. C., 2013. The Fuchuan ophiolite in Jiangnan Orogen: Geochemistry, zircon U-Pb geochronology, Hf isotope and implications for the Neoproterozoic assembly of South China. Lithos 179, 263-274. https://doi.org/10.1016/j.lithos.2013.08.015.

Zhang, J., Li, R., Pandit, M. K., Zheng, J. P., Zhao, J. H., Lan, T. G., Wang, W., 2025. Provenance variation and tectonic evolution of the Vindhyan Basin in north-central India: Implications on Proterozoic supercontinent cycles. Tectonics, 44, e2025TC009063. https://doi.org/10.1029/2025TC009063.

Zhang, Q., Zhao, L., Zhou, D., Nutman, A. P., Mitchell, R. N., Liu, Y., Li, Q. L., Yu, H. M., Fan, B., Spencer, C. J., Li, X. H., 2023. No evidence of supracrustal recycling in Si-O isotopes of Earth's oldest rocks 4 Ga ago. Sci. Adv. 9, eadf0693. https://doi.org/10.1126/sciadv.adf0693.

Zhang, S. B., Wu, R. X., Zheng, Y. F., 2012. Neoproterozoic continental accretion in South China: Geochemical evidence from the Fuchuan ophiolite in the Jiangnan orogen. Precambrian Res. 220-221, 45-64. https://doi.org/10.1016/j.precamres.2012.07.010.

Zhao, G. C., 2015. Jiangnan orogen in south china: developing from divergent double subduction. Gondwana Res. 27, 1173-1180. https://doi.org/10.1016/j.gr.2014.09.004.

Zhao, G. C., Zhang, J., Yin, C. Q., Wang, C., Zhang, G. W., 2022. Pre-Plate Tectonics and Origin of Continents. Chin. Sci. Bull. 68, 2312-2323. http://dx.doi.org/10.1360/TB-2022-0249.

Zhao, J. H., Asimow, P. D., 2014. Neoproterozoic boninite-series rocks in South China: A depleted mantle source modified by sediment-derived melt. Chem. Geol. 388, 98-111. https://doi.org/10.1016/j.chemgeo.2014.09.004.

Zhao, J. H., Zhou, M. F., Zheng, J. P., 2013. Constraints from zircon U-Pb ages, O and Hf isotopic compositions on the origin of Neoproterozoic peraluminous granitoids from the Jiangnan Fold Belt, South China. Contrib. Mineral. Petrol. 166, 1505-1519. https://doi.org/10.1007/s00410-013-0940-z.

Zhou, G. Q., Zhao, J. X., 1991. Sm-Nd isotope study of Northeastern Jiangxi ophiolite in the southeastern margin of the Yangtze Craton, South China. Chin. Sci. Bull. 36, 129-132. https://doi.org/10.1360/csb1991-36-2-129. (in Chinese)

Zhou, X. M., Zou, H. B., Yang, J. D., Wang, Y. X., 1989. Sm-Nd Isochronous Age of Fuchuan Ophiolite Suite in Shexian Country, Anhui Province and Its Geology Significance. Chin. Sci. Bull. 34, 1243-1245. https://doi.org/10.1360/csb1989-34-16-1243. (in Chinese)

Zheng, J. P., Xiong, Q., Zhao, Y., Li, W., 2019. Subduction-zone peridotites and their records of crust-mantle interaction. Sci. China-Earth Sci. 49, 1037-1058. https://doi.org/10.1007/s11430-018-9346-6.

Zheng, Y. F., 2019. Subduction zone geochemistry. Geosci. Front. 10, 1223-1254. https://doi.org/10.1016/j.gsf.2019.02.003.

Zheng, Y. F., Wu, R. X., Wu, Y. B., Zhang, S. B., Yuan, H. L., Wu, F. Y., 2008. Rift melting of juvenile arc-derived crust: geochemical evidence from Neoproterozoic volcanic and granitic rocks in the Jiangnan orogen, South China. Precambrian Res. 163, 351-383. https://doi.org/10.1016/j.precamres.2008.01.004.

Zheng, Y. F., Zhao, G., 2020. Two styles of plate tectonics in Earth's history. Sci. Bull. 65, 329-334. https://doi.org/10.1016/j.scib.2018.12.029.

Zhu, Q., Zhao, X., Hong, W., Jin, G., Huang, W., Wang, C., Liu, K., Gao, T., Wen, H., 2023. Geochronology, Hf isotope and trace element of zircon and apatite for Neoproterozoic granodiorites in the eastern Jiangnan Orogen: Implications for the Neoproterozoic tectonic evolution. Lithos 446, 107134. https://doi.org/10.1016/j.lithos.2023.107134.

Figure Captions:

Fig. 1. Simplified geological map, hand-specimen photographs and microscopic photos. (a to c) Simplified geological map of the Fuchuan Ophiolite and adjacent key Neoproterozoic igneous and sedimentary rocks in the Jiangnan Belt, South China. Modified after Huang et al. (2021) and Shu et al. (2019). (d and e) Field photographs of the Fuchuan mantle-hosted granitoids in the Fuchuan Ophiolite. (f and g) Hand-specimen photographs of the Fuchuan mantle-hosted granitoid and Shexian granitoid. The key and pen serving as scales have actual lengths of 7.1cm and 14.9cm, respectively. (h and i) Microscopic photos of the Fuchuan mantle-hosted granitoids. Abbreviation: Ap-apatite; Kfs-potassium feldspar; Mus-muscovite; Pl-plagioclase; Qz-quartz.

Fig. 2. Zircon cathodoluminescence (CL) images and U-Pb concordia diagrams. (a to d) Representative zircon CL images for sample FC19-21, FC19-22, FC10-01 and FC10-33. The white, red and yellow circles in the CL images with diameters of 54μm, 33μm and 20μm, are for Lu-Hf, U-Pb and O isotope analyses, respectively. Age, εHf(t) and $\delta^{18}O$ values of representative zircons are marked with yellow, red, and blue fonts. (e to h) Zircon U-Pb concordia plots and weighted mean ages.

Fig. 3. Bivariate plots of the selected major oxide contents/ratios against SiO_2. Data of experiment melts derived from amphibolite basalt and subduction sediment are from Johnson and Plank (1999), Rapp et al. (1991), Rushmer (1991) and Şen and Dunn (1994). Data of typical oceanic plagiogranite in the Jiangxi Ophiolite are from Gao et al. (2009), Li and Li (2003) and Sun et al. (2020).

Fig. 4. Chondrite normalized REE (a) and primitive mantle-normalized incompatible trace element (b) patterns for felsic intrusions from the Fuchuan Ophiolite. Data of Typical oceanic plagiogranite in the Jiangxi Ophiolite are from Gao et al. (2009), Li and Li (2003) and Sun et al. (2020). Leucogranite in Samail Ophiolite and Himalaya are from Guo and Wilson (2012) and Haase et al. (2015).

Fig. 5. Zircon trace elements characteristics. (a) Cumulative frequency diagrams of trace element (P and Y) concentration and ratio (U/Th) in zircon. Revised shaded areas indicating zircon provenance for I- and S-type granite in the Lachlan Fold Belt (Burnham and Berry, 2017). (b) Relationship between the concentration of P and REE+Y in magmatic zircons for I- and S-type granite.

Fig. 6. Zircon U-Pb-Hf-O isotopes. (a) $\varepsilon_{Hf(t)}$ versus $\delta^{18}O$. Green lines represent calculated mixing tend (with 10% mixing increments) between the crustal end-member (a: $\varepsilon_{Hf(t)}$ = -5.1, $\delta^{18}O$ = 11.3‰; b: $\varepsilon_{Hf(t)}$ = -2.5, $\delta^{18}O$ = 11.3‰) and the mantle end member (c: $\varepsilon_{Hf(t)}$ = +9.0, $\delta^{18}O$ = 5.6‰) (Shu et al., 2019; Zhang et al., 2012, 2013). The mantle-like zircon $\delta^{18}O$ and $\varepsilon_{Hf(t)}$ is from Valley et al. (2003), Shu et al. (2019) and Zhang et al. (2012, 2013). (b) $\varepsilon_{Hf(t)}$ versus ages. Complied data of the granitoids and basaltic rocks (Shu et al., 2019; Zhang et al., 2012, 2013), the early Neoproterozoic arc-related granitoids and plagiogranites from the eastern segment of the Jiangnan Belt (Sun et al., 2020) and the ca. 850-510 Ma strongly peraluminous granitoids (Xucun, Shexian and Jiuling plutons) (Wang et al., 2013b; Zhao et al., 2013) is shown for comparison.

Fig. 7. Th/La versus Sm/La of whole-rock geochemistry. Outline of Himalayan leucogranite and MORB are from Guillot and Le Fort (1995), Guo and Wilson (2012) and Tommasini et al. (2011). The inset diagrams show modeling of partial melting for GLOSS and the metasedimentary rocks from the Samail Ophiolite. Percentages (1%) represent the degree of partial melting. Composition of the GLOSS and metasedimentary rocks from the Samail Ophiolite are compiled from Plank and Langmuir (1998), Johnson and Plank (1999) and Rioux et al. (2021). Partition coefficients are from Hermann and Rubatto (2009) and Kessel et al. (2005). The legend is the same as that of Fig. 3.

Fig. 8. Bivariate plots of Eu/Eu* versus Rb/Sr and Ba/Sr for the Fuchuan mantle-hosted granitoids. The legend is the same as that of Fig. 3.

Fig. 9. P-T phase diagrams. Modeled P-T pseudosections for sedimentary rocks of the Xikou Group, South China (a) with 3 wt. % H_2O. The yellow dotted-dashed lines in panel (a) indicate the variation of K_2O/Na_2O value for melt. The modelling results (b, c) of phase mode (vol %) for sedimentary rocks of the Xikou Group under different geothermic gradient at 500 ℃/GPa and 1000 ℃/GPa. Composition of the sedimentary rocks of the Xikou Group (Table S5) are compiled from Xu et al. (2014).

Fig. 10. Schematic model for subduction initiation under modern plate tectonic paradigm. (a) Sinking of density and cold oceanic slab into mantle with high geotherms during subduction commencement, resulted in partial melting of sedimentary rocks on the top of subduction slab. These melts were emplaced into the shallow and cold corner of mantle wedge and solidified rapidly (this study). (b) With down-going and rollback of subduction slab, sediment-derived melts metasomatized deeper and hotter mantle peridotite and then trigger the fore-arc basaltic and boninitic magmatism in tectonic extension (Huang et al., 2021; Zhao and Asimow, 2014).

Figure 1

Click here to access/download;Figure;Figure 1.jpg

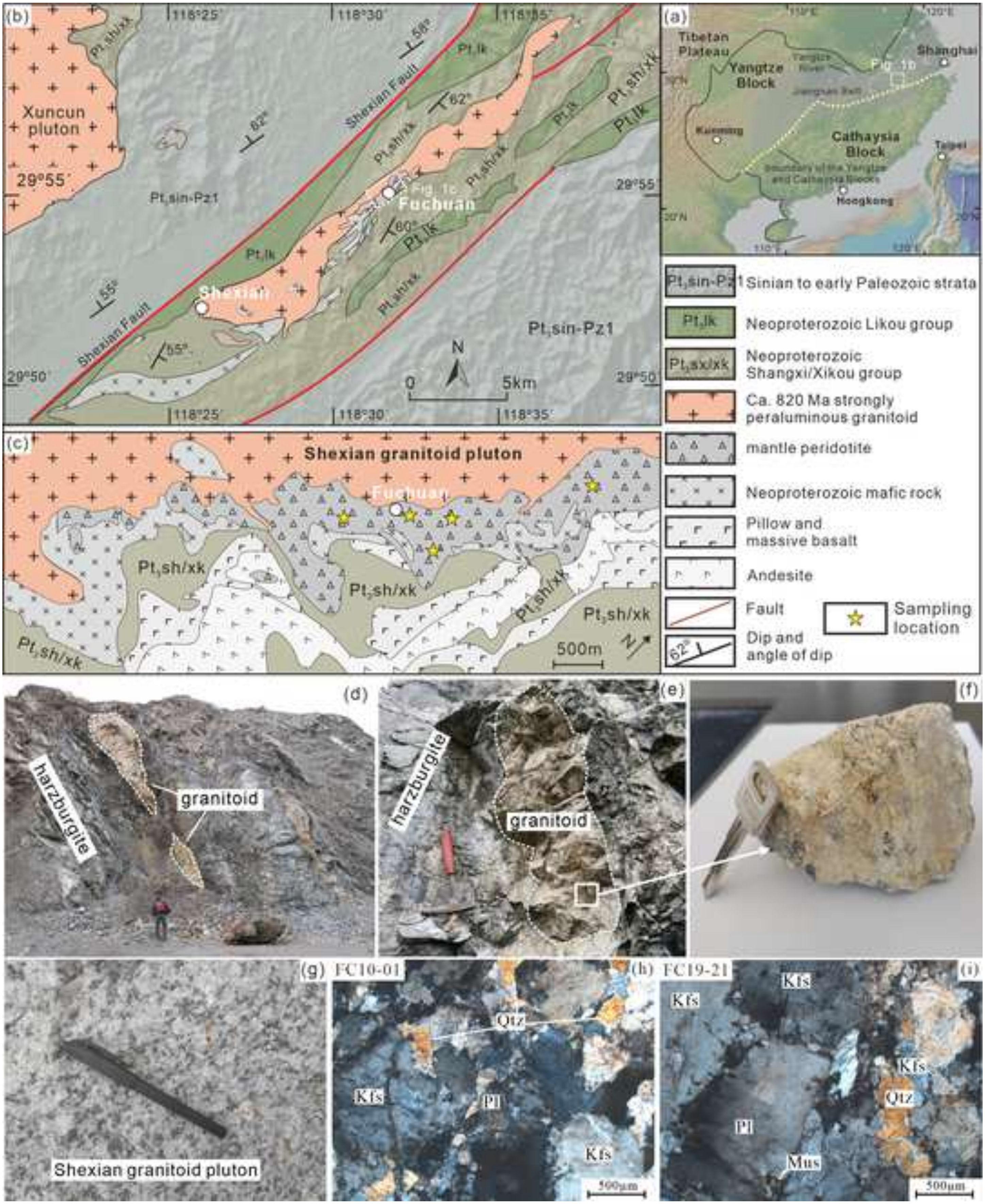

Figure 2 Click here to access/download;Figure;Figure 2.jpg

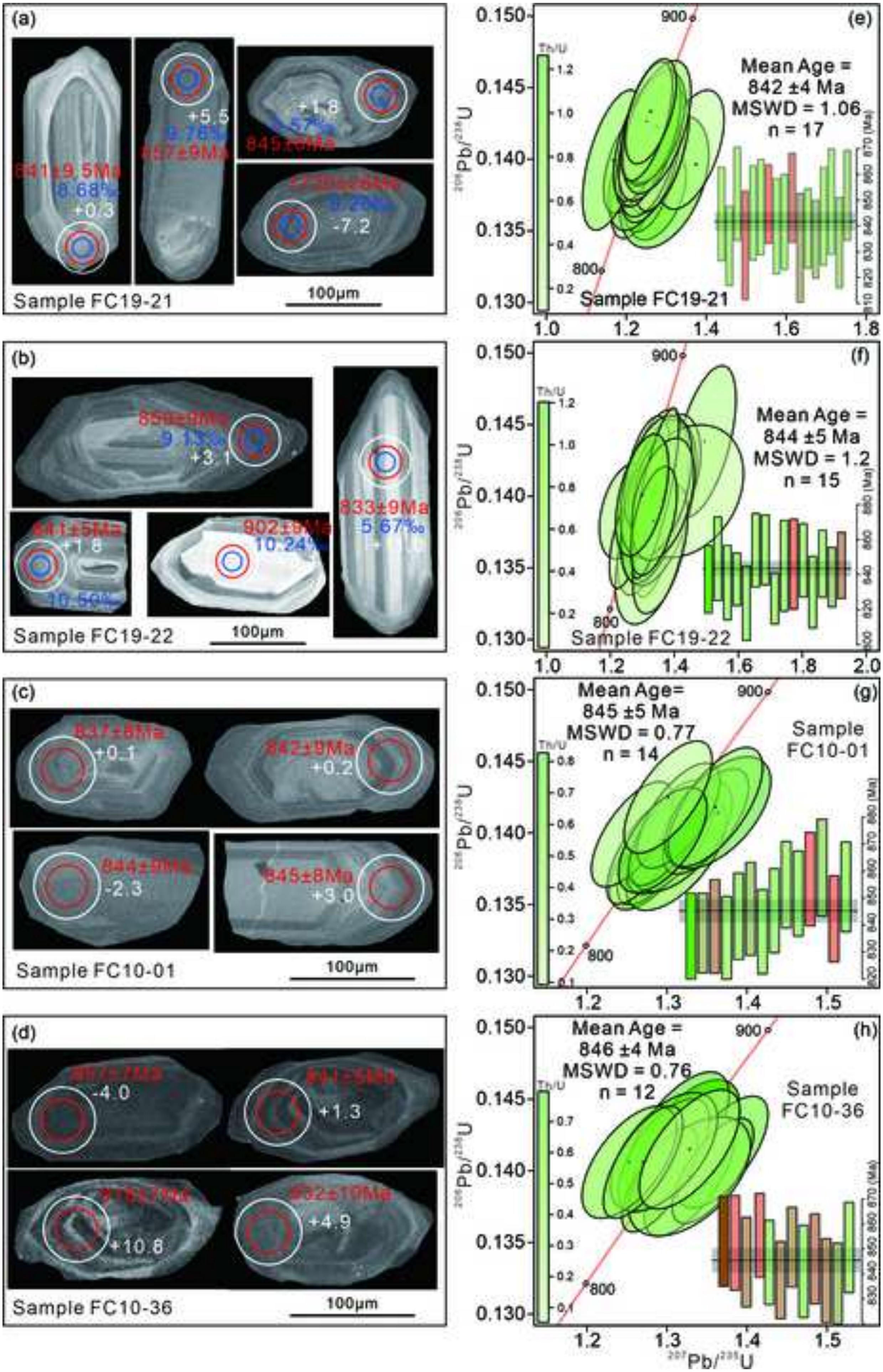

Figure 3

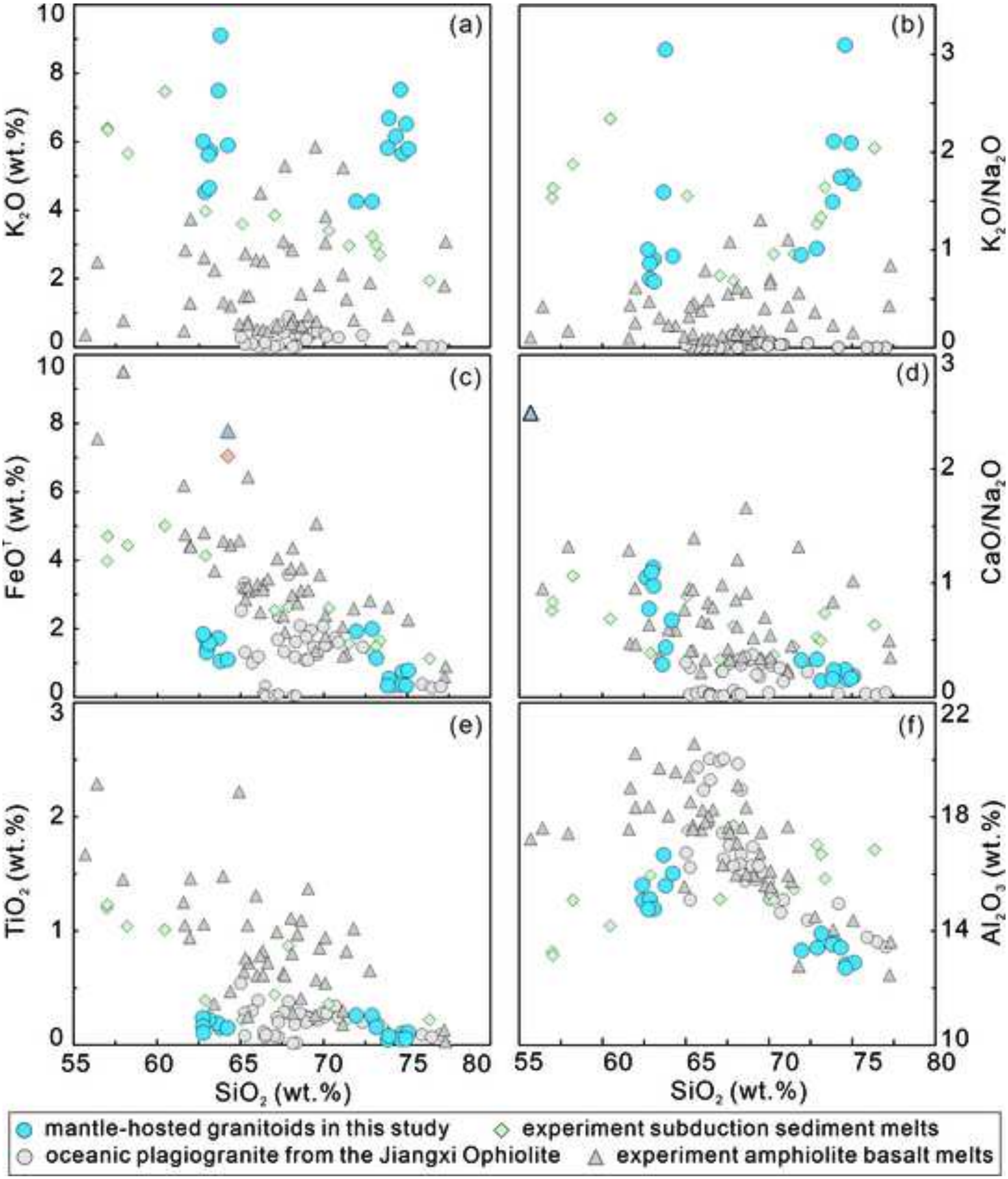

(a)
(b)
(c)
(d)
(e)
(f)
K2O (wt.%)
K2O/Na2O
FeOT (wt.%)
CaO/Na2O
TiO2 (wt.%)
Al2O3 (wt.%)
SiO2 (wt.%)
SiO2 (wt.%)
mantle-hosted granitoids in this study
experiment subduction sediment melts
oceanic plagiogranite from the Jiangxi Ophiolite
experiment amphiolite basalt melts

Figure 4

Click here to access/download;Figure;Figure 4.jpg

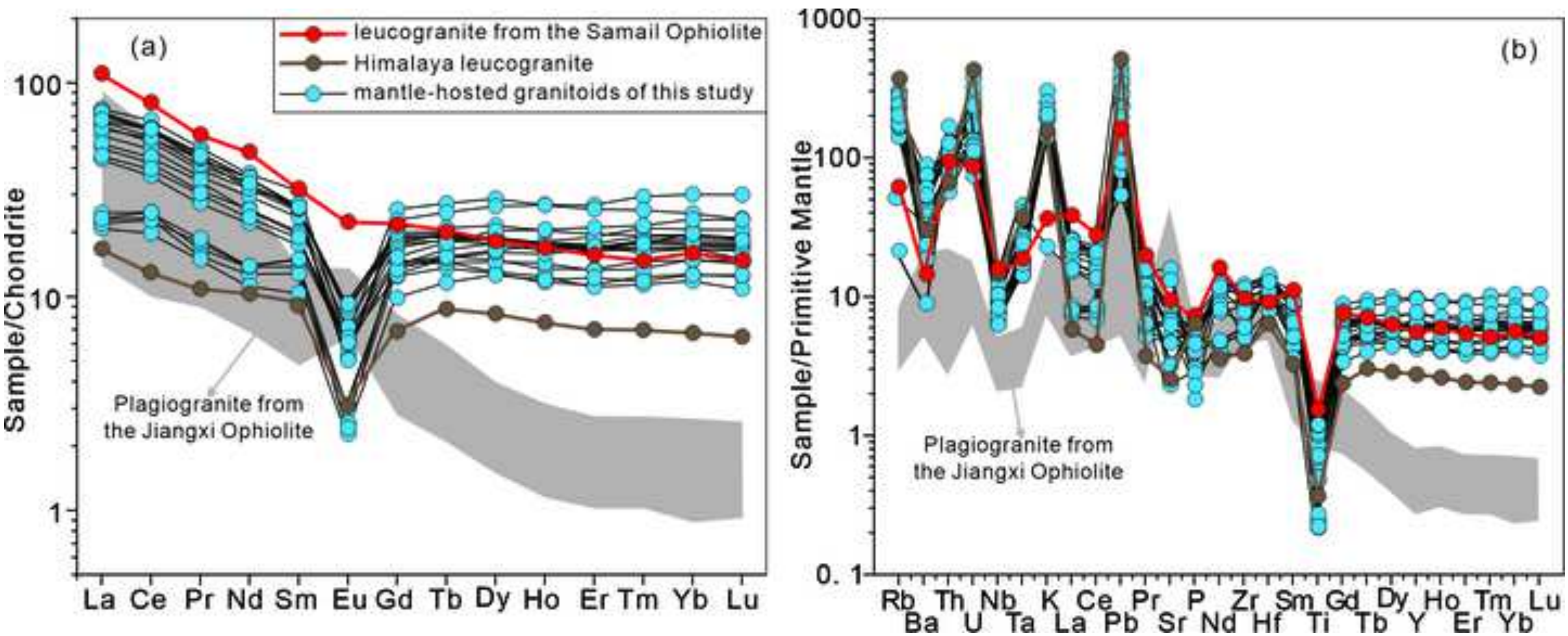

Figure 5

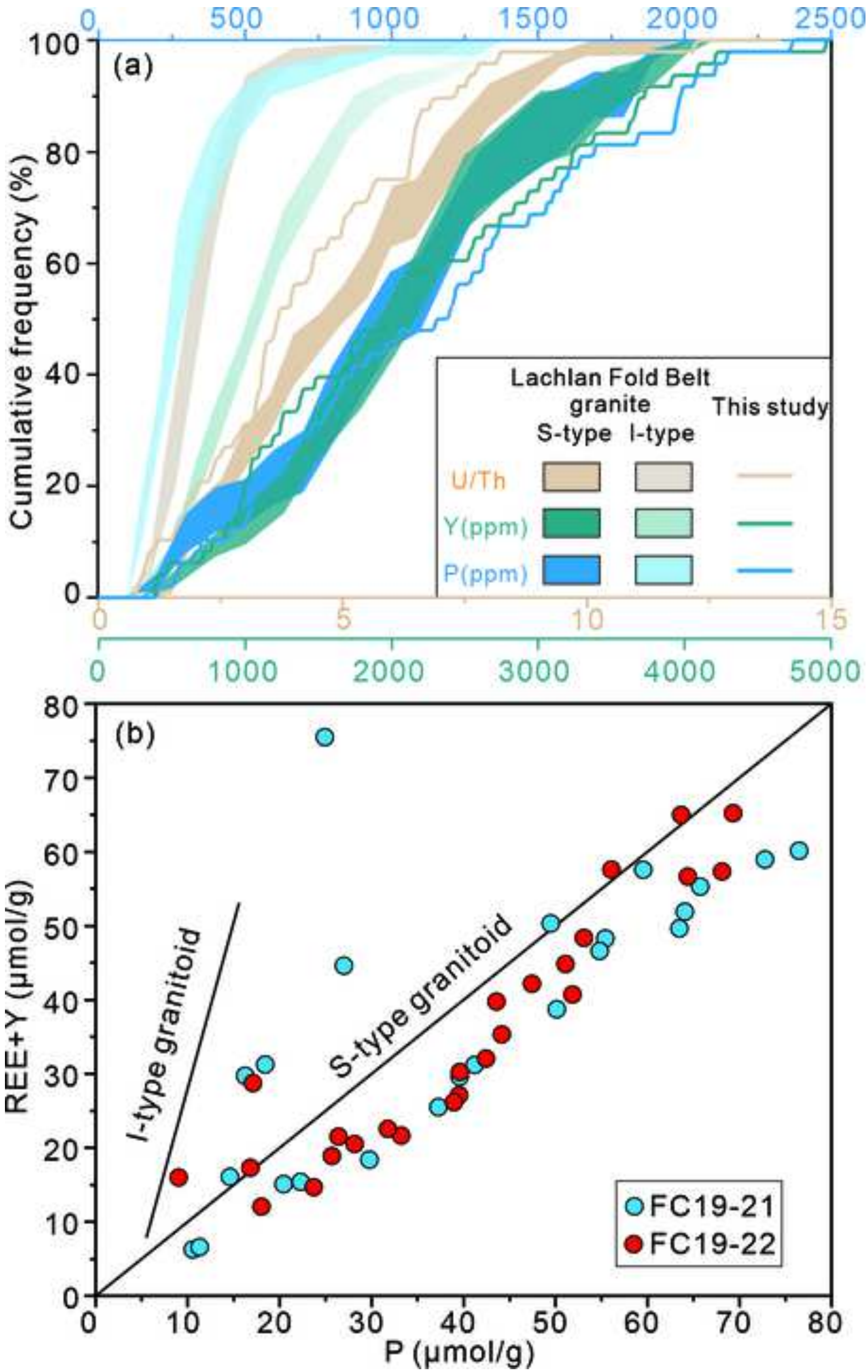

(a)
Cumulative frequency (%)
Lachlan Fold Belt granite
S-type
I-type
This study
U/Th
Y(ppm)
P(ppm)
(b)
REE+Y (μmol/g)
P (μmol/g)
I-type granitoid
S-type granitoid
FC19-21
FC19-22

Figure 6 Click here to access/download;Figure;Figure 6.jpg

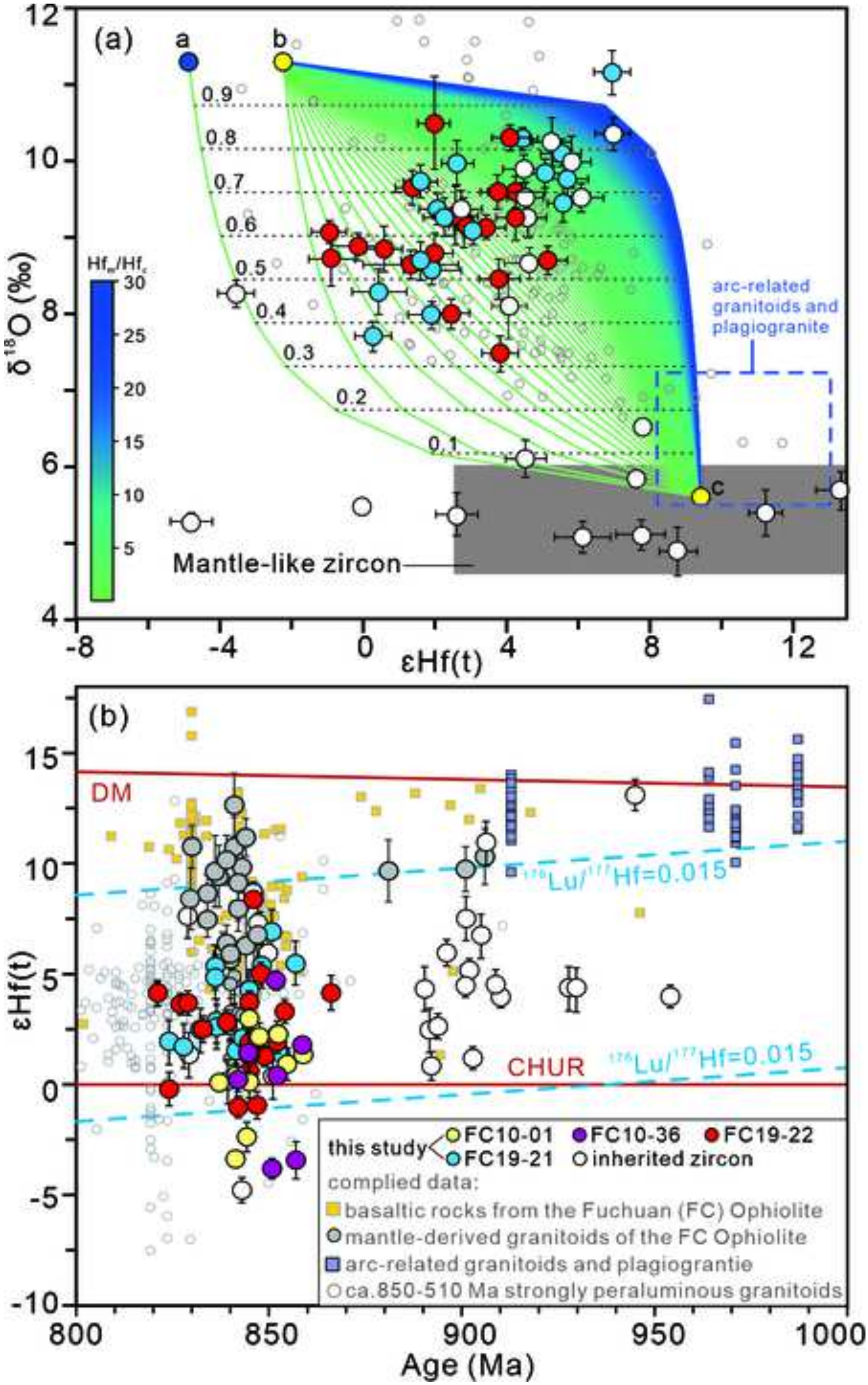

Figure 7

Click here to access/download;Figure;Figure 7.jpg

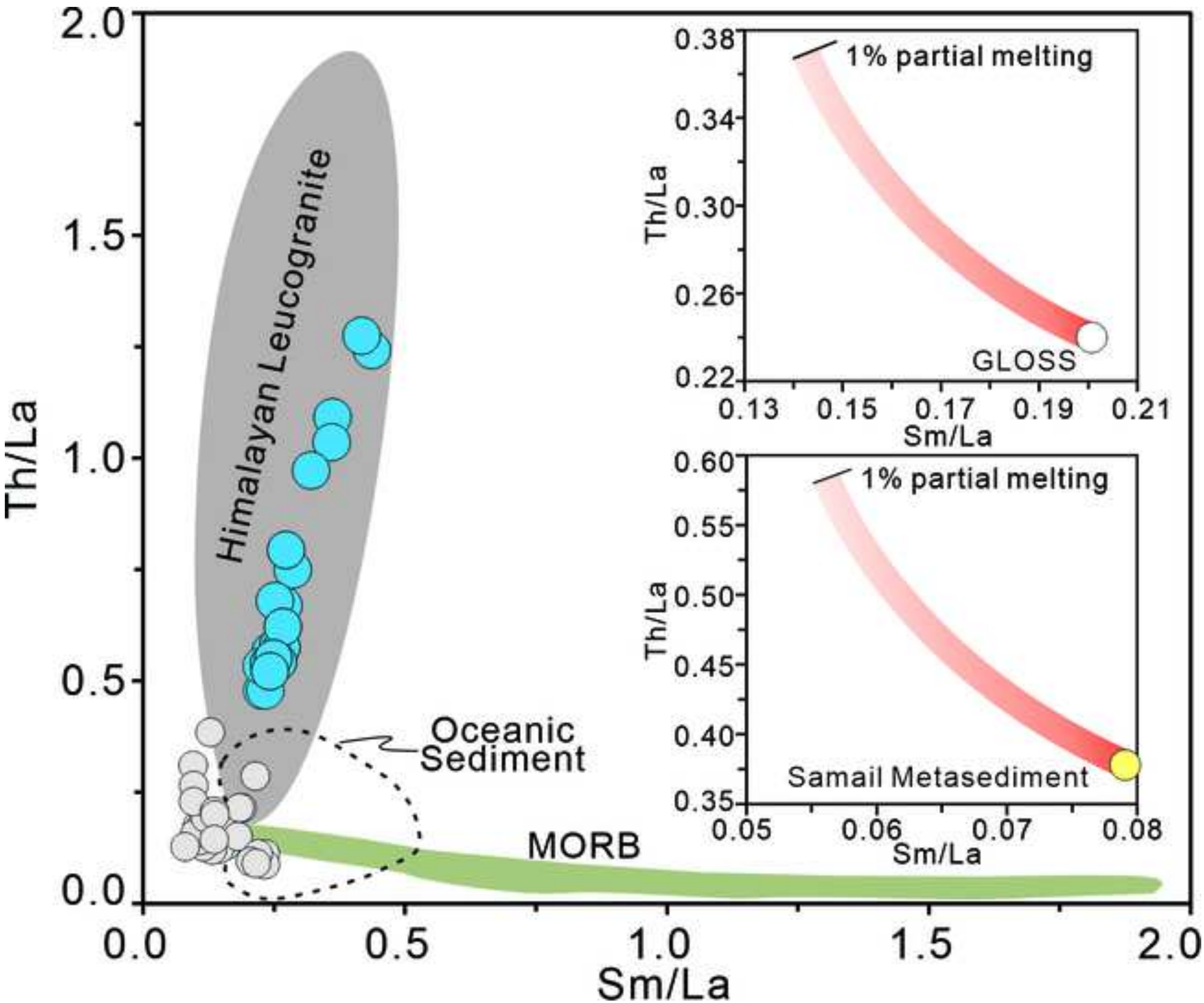

Figure 8

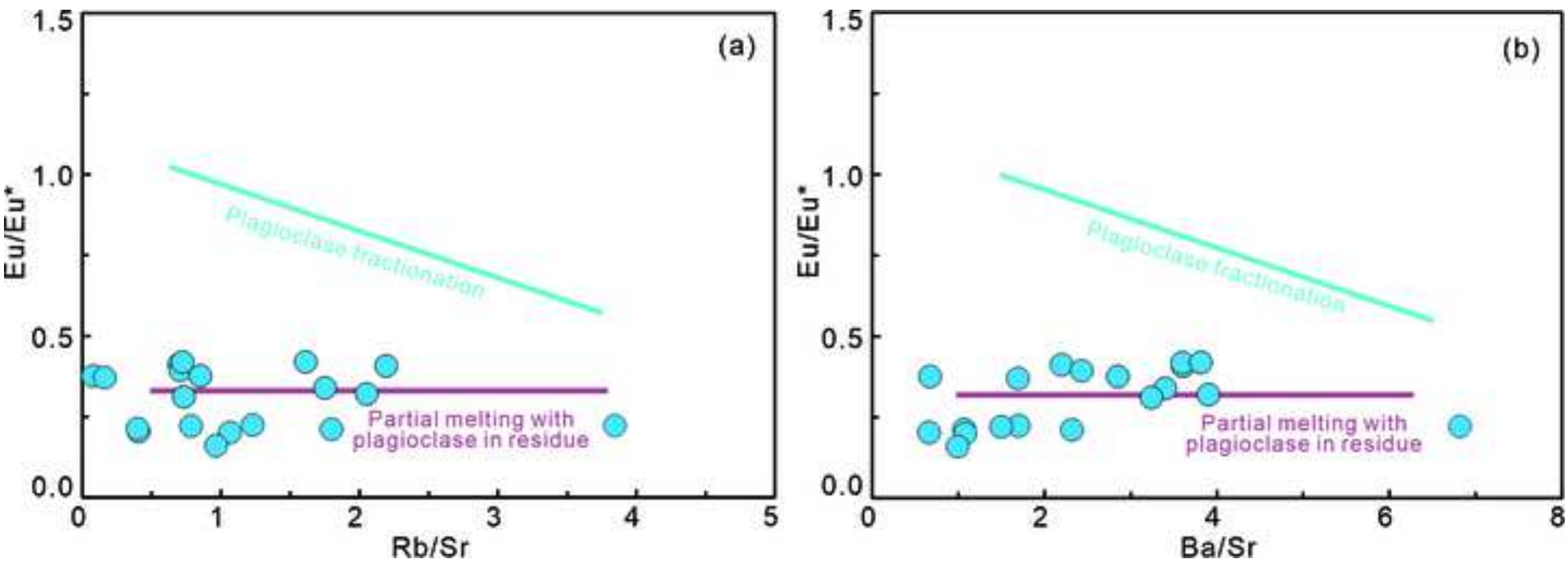

(a)
Eu/Eu*
1.5
1.0
0.5
0.0
0
1
2
3
4
5
Rb/Sr
Plagioclase fractionation
Partial melting with plagioclase in residue
(b)
Eu/Eu*
1.5
1.0
0.5
0.0
0
2
4
6
8
Ba/Sr
Plagioclase fractionation
Partial melting with plagioclase in residue

Figure 9

Click here to access/download;Figure;Figure 9.jpg

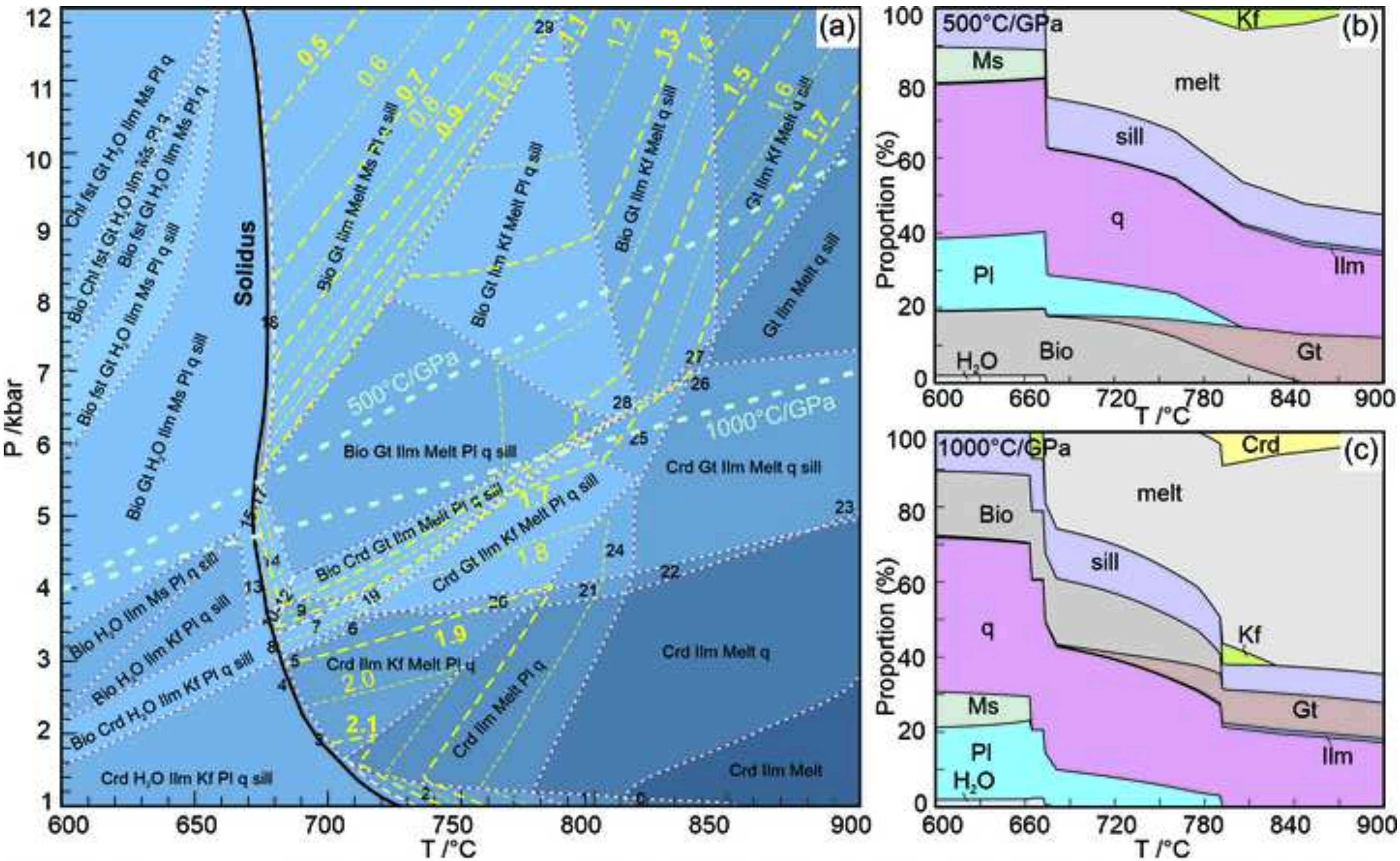

0 Crd H_2O Ilm Melt
1 Crd H_2O Ilm Melt q
2 Crd H_2O Ilm Melt Pl q
3 Crd H_2O Ilm Kf Melt Pl q
4 Crd H_2O Ilm Kf Melt Pl q sill
5 Bio Crd H_2O Ilm Kf Melt Pl q sill
6 Crd Ilm Kf Melt Pl q sill
7 Bio Crd Ilm Kf Melt Pl q sill
8 Bio Crd Gt H_2O Ilm Kf Melt Pl q sill
9 Bio Crd Ilm Melt Pl q sill
10 Bio Crd H_2O Ilm Melt Pl q sill
11 Bio Crd Gt H_2O Ilm Kf Pl q sill
12 Bio Crd Gt H_2O Ilm Melt Pl q sill
13 Bio Gt H_2O Ilm Kf Pl q sill
14 Bio Gt H_2O Ilm Melt Pl q sill
15 Bio Gt H_2O Ilm Kf Melt Pl q sill
16 Bio H_2O Ilm Kf Ms Pl q sill
17 Bio Gt H_2O Ilm Kf Ms Pl q sill
18 Bio Gt H_2O Ilm Melt Ms Pl q sill
19 Bio Crd Gt Ilm Kf Melt Pl q sill
20 Crd Gt Ilm Kf Melt Pl q
21 Crd Gt Ilm Melt Pl q
22 Crd Gt Ilm Melt q
23 Crd Ilm Melt q sill
24 Crd Gt Ilm Melt Pl q sill
25 Crd Gt Ilm Kf Melt q sill
26 Bio Crd Gt Ilm Melt q sill
27 Bio Gt Ilm Melt q sill
28 Bio Crd Gt Ilm Kf Melt q sill
29 Bio Gt Ilm Kf Melt Ms q sill

(a) Sediment melts immediately when subduction initiation and then intrude into the cold corner of mantle wedge

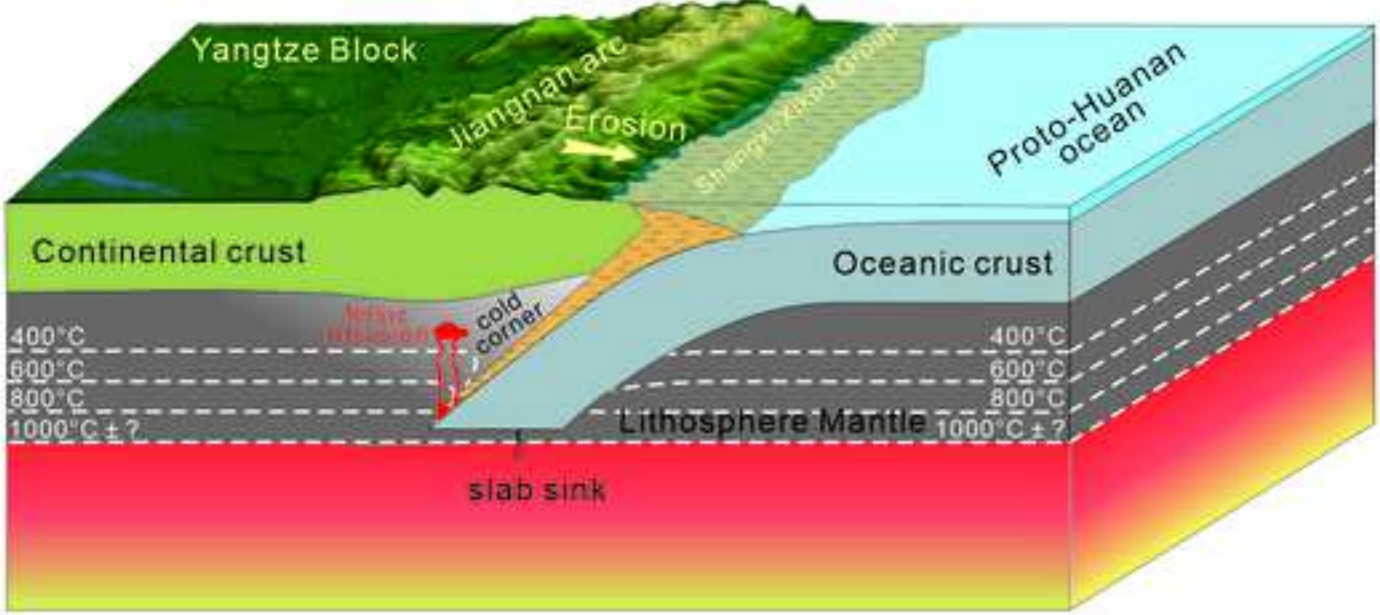

(b) With down-goning of slab, fore-arc extension trigger boninitic magmatism in the slightly deeper mantle

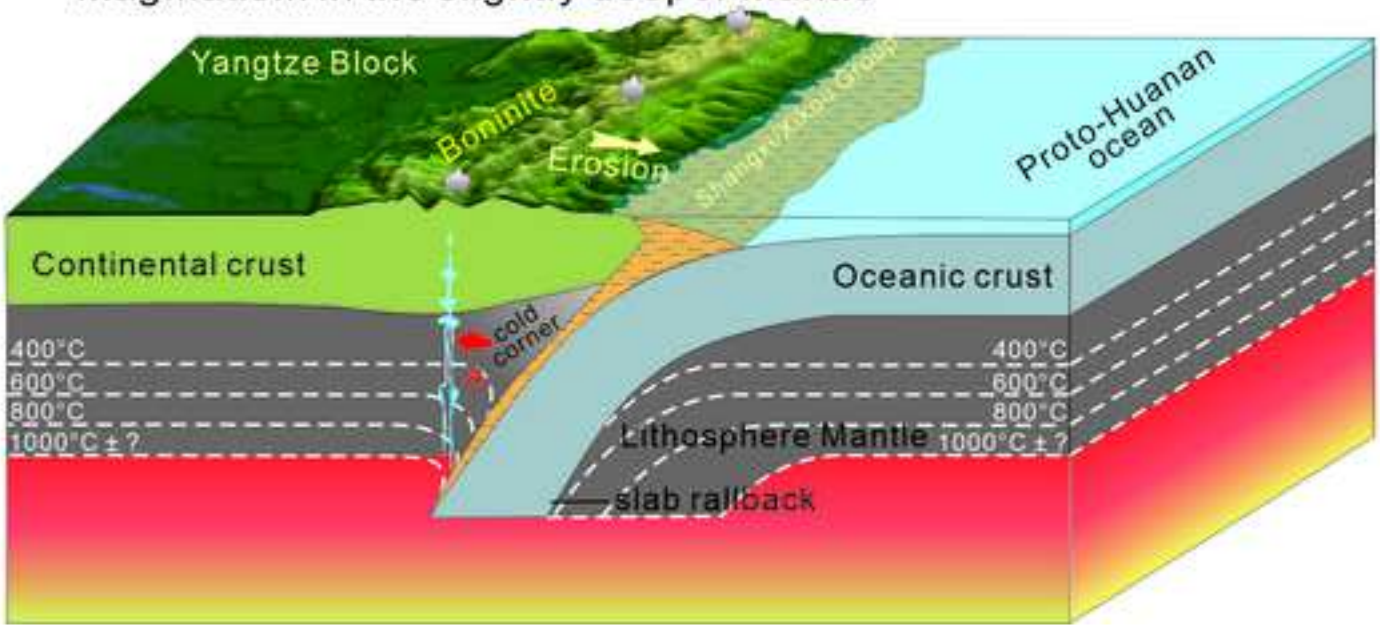

Supplementary tables

Click here to access/download
e-Component
Supplementary Tables.xls

Click here to access/download
e-Component
Supplementary Information.docx